2020

Particle formation and surface processes on atmospheric aerosols: a review of applied quantum chemical calculations

George C. Shields
Furman University

Ariel Gale

Tyler Ball

Tuguldur T. Odbadrakh
Furman University

Angelini Leonardi
Skidmore College

See next page for additional authors

Received: 8 April 2020 | Revised: 8 May 2020 | Accepted: 26 May 2020

DOI: 10.1002/qua.26350

REVIEW

International Journal of Quantum Chemistry WILEY

Particle formation and surface processes on atmospheric aerosols: A review of applied quantum chemical calculations

Angelina Leonardi[1] | Heather M. Ricker[1] | Ariel G. Gale[2] | Benjamin T. Ball[2] | Tuguldur T. Odbadrakh[2] | George C. Shields[2] | Juan G. Navea[1]

[1]Chemistry Department, Skidmore College, Saratoga Springs, New York, USA

[2]Department of Chemistry, Furman University, Greenville, South Carolina, USA

Correspondence
Juan G. Navea, Chemistry Department, Skidmore College, Saratoga Springs, NY 12866-1632.
Email: jnavea@skidmore.edu

George C. Shields, Department of Chemistry, Furman University, Greenville, SC 29613.
Email: george.shields@furman.edu

Funding information
National Science Foundation, Grant/Award Numbers: CHE-1229354, CHE-1662030, CHE-1721511, CHE-1903871; Schupf Scholar Program (AL); Barry M. Goldwater Scholarship (AGG); Arnold and Mabel Beckman Foundation Beckman Scholar Award (AGG); NSF Center for Aerosol Impacts on Chemistry of the Environment (CAICE), Grant/Award Numbers: DBI-1828508, CHE-1801971

Abstract

Aerosols significantly influence atmospheric processes such as cloud nucleation, heterogeneous chemistry, and heavy-metal transport in the troposphere. The chemical and physical complexity of atmospheric aerosols results in large uncertainties in their climate and health effects. In this article, we review recent advances in scientific understanding of aerosol processes achieved by the application of quantum chemical calculations. In particular, we emphasize recent work in two areas: new particle formation and heterogeneous processes. Details in quantum chemical methods are provided, elaborating on computational models for prenucleation, secondary organic aerosol formation, and aerosol interface phenomena. Modeling of relative humidity effects, aerosol surfaces, and chemical kinetics of reaction pathways is discussed. Because of their relevance, quantum chemical calculations and field and laboratory experiments are compared. In addition to describing the atmospheric relevance of the computational models, this article also presents future challenges in quantum chemical calculations applied to aerosols.

KEYWORDS

adsorption, heterogeneous chemistry, prenucleation, secondary organic aerosol, surface

1 | INTRODUCTION

Atmospheric aerosols, also known as particulate matter (PM), are suspensions of liquid or solid particles in the atmosphere with a wide variation in composition and size. An aerosol is technically defined as a suspension of fine solid or liquid particles in a gas, but its use in atmospheric chemistry usually refers only to the particulate component. Particles emitted directly as particles are called primary aerosols, while particles formed by gas-to-particle conversion in the atmosphere are called secondary aerosols. The concentrations of aerosol particles can be as high as 10^6 to 10^7 cm^{-3}, and the diameters of these particles range over four orders of magnitude, from a few nanometers (nm) upwards to 100 μm. This size range is so vast that a billion particles with a diameter of 10 nm have the same mass as one particle with a diameter of 10 μm. This tremendous size range makes accounting for all particles in the atmosphere that could be called an aerosol quite challenging.[1]

The interfacial system of atmospheric aerosols is highly complex, as the properties of aerosol particles depend on multiple variables controlling their formation and their atmospheric processing. For instance, atmospheric aerosols may be emitted directly from natural or anthropogenic sources (primary aerosol) or generated in situ from the chemical and physical changes during the processing of gaseous precursors (secondary aerosol). Figure 1 shows several examples of primary aerosols, with differences in size and chemical composition that lead to large uncertainties in their effects on climate, health, and the overall Earth system. Because of their relatively small size (2 nm to 10 μm), atmospheric aerosols have little inertia and can remain suspended for several days, resulting in long-range transport and significant impact in the chemical balance of the

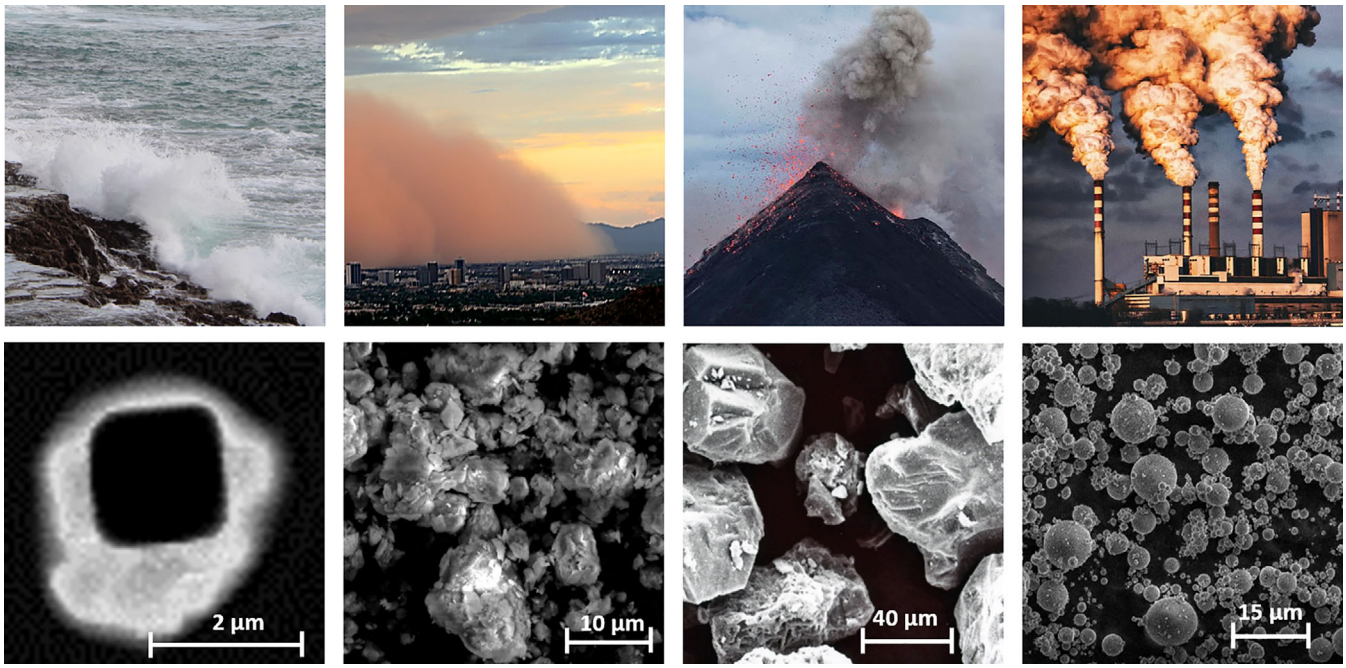

FIGURE 1 Top: Sea-spray aerosol, desert-sand dust, volcanic ash, and fly ash are sources of aerosols (photographs under Creative Commons). Bottom: Matching scanning electron microscope images (not at the same scale) showing the wide variety of aerosol sizes and shapes. Micrographs courtesy USCD/NSF-CAICE (Vicki H. Grassian) and Skidmore College/NSF-CAICE (Juan G. Navea)

atmosphere.[1,2] In fact, recent laboratory and modeling studies have shown that PM has important implications in biogeochemical cycles,[3–10] heavy-metal transport,[11,12] cloud nucleation,[13–17] and heterogeneous reactions,[18–26] among other direct or indirect impacts.

Over the last two decades, a great deal of effort has been made to address the formation, evolution, and impacts of various aerosols. In particular, the increase of computing power and deeper experimental examination of the chemistry and physics that drive atmospheric processes have allowed computational methods to advance our understanding of aerosol impacts on the chemistry of trace atmospheric gases and pollutants, as well as climate in general. First, on a macroscopic level, box modeling has been used to assess the impact of aerosol particles on climate, biogeochemical cycles, and the lifetime of potential pollutants.[24,27] Second, molecular dynamics (MD) simulations have been successfully implemented to model physicochemical phenomena such as ice nucleation on sea-spray aerosols and water coverage mobility on atmospheric aerosols.[28–31] While these two approaches are paramount to understanding the chemistry of aerosols as it pertains to climate and the environment, recent work has required the use of quantum mechanical (QM) methods to advance our understanding of aerosol phenomena at a molecular level.

The complexity of atmospheric aerosol studies arises from the wide range of chemical compositions known to provide active surface sites for the adsorption of trace atmospheric gases, with the concomitant impact on aerosols sources, particle lifetime, climate, and interaction with sunlight.[18,32] Quantum chemical calculations provide a molecular understanding of aerosol phenomena by aiding the interpretation of laboratory experiments or by providing stand-alone models that allow for building complexity. Quantum chemical calculations have been used to understand atmospheric aerosol particles in two broadly defined systems: (a) homogeneous chemistry, in which the formation of PM from gas-phase or solution-phase species are modeled (eg, prenucleation, gaseous reactions leading to secondary aerosol formation, and chromophore adsorption cross-sections), and (b) interface chemistry involving surface chemistry (eg, surface-bound molecules leading to the formation or growth of atmospheric particles, adsorption of trace atmospheric gases onto aerosol surfaces, and spectroscopic simulations of atmospheric trace gases adsorbed onto components of atmospheric particles). Given the substantial amount of work available on box modeling and MD methods involving PM, here we briefly synthesize the current state of knowledge of QM methods applied to the chemistry of aerosol particles. In particular, this work emphasizes recent progress in prenucleation, secondary organic aerosol (SOL) formation, surface chemistry, and photochemistry.

2 | PARTICLE FORMATION

Without aerosols, there would be no clouds, as these particles serve as the nuclei that stimulate the formation of clouds. Particles that become activated to grow to clouds or fog in the presence of a supersaturation of water vapor (ie, saturation (S) >1; or relative humidity (RH) > 100%) are

called cloud condensation nuclei.[1] Prenucleation is a process that occurs all the time as gas molecules continually add to or leave a particular secondary aerosol cluster. Sulfuric acid is one of the most important precursors of secondary aerosol in the atmosphere. Gaseous sulfuric acid in small amounts is able to induce nucleation in the air even when the RH is less than 100%,[33] and for this reason is one of the most studied systems. Details of quantum mechanics applied to the study of prenucleation are outlined below.

2.1 | Prenucleation through quantum chemistry

As mentioned in the Introduction, the sizes of aerosol particles range from nanometers to micrometers, with concentrations as high as 10^6 to 10^7 cm^{-3}. In principle, we could refer to two gas-phase molecules that are stuck together by intermolecular forces as the smallest aerosol, or any integer number n of molecules held together as an aerosol.[1] Many small molecules, such as water, acids, bases, and organic compounds, exist in both gas and aerosol phases in the atmosphere. Gas-phase molecules form clusters by the addition of one molecule to the cluster at a time, and they also lose molecules one at a time, so the atmosphere is filled with rapidly growing and shrinking gas-phase clusters. These small clusters can be scavenged by large aerosols or potentially grow to become new aerosol particles. The latter is an atmospheric new particle formation preceded by the aggregation of gaseous molecules from random collisions to form "prenucleation clusters," which is held together through long-range noncovalent interactions between the constituent gas molecules.[1,33–35] Overall, the concentration of gaseous monomers always exceeds the concentration of all other clusters combined. Once the gas vapor becomes saturated (S = 1), the average concentration of all clusters at saturation equilibrium is constant. At a level of saturation greater than 100% (S > 1, or RH >100% for water vapor), the excess of monomer molecules increases the size and number of clusters that existed when S = 1. At a large value of S, some of the largest clusters exceed a critical size, such that they can now grow rapidly into cloud condensation nuclei and form a new phase. The "critical cluster" has a steady-state size, with the nucleation rate as the net number of clusters that grow past the critical size.[1]

Classical nucleation theory uses bulk properties to simulate the growth of aerosols. This approach requires two basic assumptions: first, an isobaric transfer of gaseous molecules into liquid phase, and second, gaseous molecules separate from the liquid phase. The first step has a Gibbs free energy change of zero, since the two phases are at saturation equilibrium, but the second step creates an interface between the gas and liquid that has a free energy change based on the surface tension of the solute and the surface area of the cluster. The two assumptions, namely (a) the surface tension of small clusters is the same as the surface tension of the liquid, and (b) the surface area of a cluster is derived assuming that the cluster is spherical, do not hold for small clusters. One result of using macro properties to describe a nano-sized system is that classical binary H_2SO_4–H_2O homogeneous nucleation theory underpredicts atmospheric observations by over 10 orders of magnitude.[1] Much of this discrepancy is due to the defects in the macro theory, and the rest of it is because base species and potentially other molecules also play a role in sulfuric acid nucleation.

An alternative to classical theory is to use quantum chemistry to obtain a detailed understanding of the growth of small gas-phase clusters to prenucleation clusters. These prenucleation molecular clusters have diameters on the order of 1–10 nm and may be composed of a single species (homomolecular) or multiple species (heteromolecular) of gases.[36] For homogenous systems without phase boundaries to act as a substrate for nucleation, only heteromolecular prenucleation clusters lead to eventual new particle formation. In fact, experiments showed as early as 1881 that homomolecular clusters, namely water, require such high supersaturations of the molecular gas species that it is impossible to form aerosols in in a homogenous medium.[37] As such, computational models of prenucleation have focused on heteromolecular processes in a homogenous medium in order to acquire physical and mechanistic insights at the molecular level. Although the dynamics and bulk properties of prenucleation cluster formation can be accessed through classical MD simulations, detailed molecular-level understanding of cluster formation requires a QM description of the underlying physics. In this field, density functional theory (DFT)[38,39] has been the dominant quantum chemistry method because of its low computational cost compared to correlated wavefunction-based methods such as Moller–Plesset perturbation theory (MPn),[40] configuration interaction,[41] and coupled-cluster (CC).[42] Of the correlated methods, the second-order Moller–Plesset perturbation theory (MP2) is utilized most because of its relatively favorable cost, and further reduction in cost using density-fitting (DF-MP2),[43] resolution of identity (RI-MP2),[44] and their combinations makes it possible to treat large clusters at reasonable chemical accuracy. MP2 is particularly good for pure water clusters[45–48] but overestimates the all-important long-range dispersion interactions for heterogeneous systems, thus requiring parameterized dispersion corrections.[49,50] High-level model chemistries such as G3, CBS-QB3, and CBS-APNO have been quite successful for looking at small clusters and gas-phase reactions.[51,52] DFT requires parameterized dispersion corrections, but offers the advantage of lower computational cost. Hence, DFT has been the main tool of quantum chemists to study gas-phase molecular clusters and their implications in new particle formation and atmospheric aerosol chemistry. We now present recent advances in the application of these quantum chemistry methods to the study of prenucleation clusters.

In order to extract the parameters needed for nucleation models from quantum chemistry calculations, one must first identify the low-energy isomers of the prenucleation clusters. This is not a trivial undertaking, as the number of possible conformations of a cluster ensemble increases dramatically as the number of monomers in the system increases.[53] To this end, many configurational sampling methods have been developed. Past studies have employed manual construction guided by chemical intuition,[54] random sampling,[55–58] basin hopping (BH),[53,59] and frozen

geometries extracted from MD[46,60–65] and Monte Carlo (MC)[66,67] simulations. Configurational sampling has recently benefited from various applications of genetic algorithms (GA).[68–76] Temelso et al used the OGOLEM implementation of GA to characterize ternary prenucleation clusters[77] and glycine–water clusters.[78] The artificial bee colony (ABC) algorithm has recently been employed extensively to study atmospherically relevant clusters.[79–84] Recently, a new systematic method of configurational sampling based on the Fibonacci sphere has been applied to atmospheric molecular clusters.[85,86] Once all the low-energy isomers are identified by one of these configurational sampling methods,[87] the main parameter of interest to be computed using quantum chemistry is the equilibrium constant of formation under atmospherically relevant conditions dictated by the temperature, pressure, and RH. This is accomplished by computing finite-temperature corrections to the gas-phase vacuum energy of the molecular cluster and involves the computation of the vibrational structure of the cluster, so that the Gibbs free energy of formation can be calculated at the desired temperature. Temperatures in the troposphere range from 298 K on Earth's surface down to 217 K at the top of the troposphere.[1]

Atmospheric aerosol formation has been tied to gaseous hydrated sulfuric acid (H_2SO_4) since early studies by Doyle et al[88] and has been the focus of many subsequent atmospheric measurements and laboratory experiments.[36,89–99] The ability of H_2SO_4 to form strong hydrogen bonds to water molecules,[100,101] its low vapor pressure,[89,102] and significant atmospheric concentration[103] make it the main driver of new particle formation, and early studies focused on the precursor clusters of binary nucleation of H_2SO_4. RI-MP2 electronic structure at the complete basis set (CBS) limit combined with anharmonic vibrational frequencies from either second-order vibrational perturbation theory (VPT2) or scaled harmonic values suggests that a single H_2SO_4 molecule at room temperature may form stable prenucleation clusters with up to four water molecules, while the H_2SO_4 dimer can accommodate up to five water molecules.[65,100] However, the thermodynamic unfavorability of accommodating more than four or five water molecules suggests that the purely binary H_2SO_4–H_2O system lacks the binding strength to lead to new particle formation. Recent systematic studies of gas-phase bimolecular H_2SO_4–X clusters, where X are hydrogen-bond acceptors, have revealed that the binding strength is a function of the energy gap between the lowest unoccupied molecular orbital (LUMO) of H_2SO_4 and the highest occupied molecular orbital (HOMO) of X.[104,105] It was shown that a smaller energy gap results in a stronger hydrogen bond. Methylation of X lowers the energy gap and can lead to the deprotonation of H_2SO_4, which suggests that increasing the basicity of the interacting molecules stabilizes the bimolecular H_2SO_4–X cluster.[106,107] In fact, this effect was observed in various studies of the precursor clusters of ternary nucleation where atmospheric amines were added to the H_2SO_4–H_2O system.[107]

The stabilizing effect of adding ammonia (NH_3) to the H_2SO_4–H_2O system has long been known and has been studied both in laboratory experiments[98,108–111] and theoretical models.[107,112] The H_2SO_4– H_2O–NH_3 system is thought to be an important precursor to ternary nucleation events leading to new particle formation. Furthermore, alkylamines have been shown to stabilize H_2SO_4–H_2O clusters. A recent study examined the effect of mixing ammonia and various alkylamines on sulfate aerosol formation and concluded that gas-phase basicity of the bases in a cluster is the main determinant of binding strength in smaller clusters, while aqueous-phase basicity is more important for larger particles.[77] This finding is in agreement with a field campaign over polluted cities in China, where it was discovered that sulfuric acid dimers bind more tightly to dimethylamine than to other bases.[99]

Ion-induced nucleation is another potential pathway to grow clusters, and the presence of ions has been shown experimentally to enhance the rate of nucleation.[113] The CLOUD chamber experiments at CERN revealed that ion-induced nucleation of pure organic particles constitutes a potentially widespread source of aerosol particles in terrestrial environments with low sulfuric acid pollution.[114] Very high level quantum chemistry methods reveal that clusters of water around OH^-, $H_2SO_4^-$, H_3O^+, and NH_4^+ ions will all have at least one full shell of water around each ionic core.[115–118] So, for instance, for a system consisting of NH_4^+ and up to 10 water molecules, if we use a concentration for NH_4^+ of 1.02×10^{-10} M (quite common above industrial pig farms)[119] and a water concentration of 1.30×10^{-3} M (S = 1 at 298 K), then we can solve the 10 simultaneous equations for

$$NH_4^+ + (H_2O)_{n-1} \rightleftarrows NH_4^+(H_2O)_n \quad (1)$$

when n = 1–10. Using MP2 calculations extrapolated to the CBS limit reveals that only 10^2 NH_4^+ cm^{-3} remains unhydrated, with the greatest concentrations at hydration levels n = 4–5, and a maximum of 4.90×10^{10} $NH_4^+(H_2O)_4$ clusters per cm^3. The numbers of clusters with n = 3 and n = 6 are on the order of 10^8 cm^{-3} under these conditions. Further up in the troposphere, as the temperature falls to 242 K, the water concentration drops to 2.39×10^{-5} M. However, the Gibbs free energies for these 10 clustering reactions become more negative, such that the estimated amount of free NH_4^+ decreases to 2 cm^{-3}, and the maximum concentrations are 5.34×10^{10} for $NH_4^+(H_2O)_4$ and 7.71×10^9 for $NH_4^+(H_2O)_5$.[117] We expect that these results can be generalized to the saturation of any ion in the atmosphere with 1–6 water molecules.[115–118] Ion-induced nucleation is the dominant process over large regions of the troposphere where particle formation rates are low,[98] but recent experimental evidence suggests that they are scavenged relatively quickly by other particles in polluted urban atmospheres.[99]

Indeed, the high relative concentration of water vapor in the atmosphere, at any typical level of RH, means that water molecules outnumber other molecular concentrations by many orders of magnitude. This results in some level of hydration for most gas-phase molecules. So, for instance, MP2 calculations reveal that the Gibbs free energies of formation for $HO_2(H_2O)_{n\,=\,1-2}$ clusters are slightly negative, leading to the prediction that when the HO_2 concentration is on the order of 10^8, and S = 1 (100% RH) at 298 K, we would expect to have 10^7 $HO_2(H_2O)$ clusters

and 10^6 $HO_2(H_2O)_2$ clusters.[119] The hydroxyl radical itself should also always be solvated, given that when the concentration of this radical is 1.66058×10^{-14} M (10^7 cm^{-3}), and S = 1 at 298 K, G3 model chemistry leads to the prediction that the concentration of $OH(H_2O)$ is 10^4.[120] An increase in the local OH concentration by a factor of 1000 would then produce 10^7 solvated hydroxyl clusters on a warm humid day. Even nonpolar molecules such as carbon disulfide will form clusters with water when their concentrations are high enough. The MP2/aug-cc-pVTZ Gibbs free energy of formation for $CS_2(H_2O)$ is 3 kcal mol^{-1}, and for the stepwise addition of a second water molecule to form $CS_2(H_2O)_2$ it is 2.5 kcal mol^{-1}. Assuming an atmospheric abundance of 1.91×10^9 cm^{-3} leads to a prediction of 10^5 $CS_2(H_2O)$ and 10^2 $CS_2(H_2O)_2$ clusters when S = 1 at 298 K.[121] Carbon disulfide is quickly oxidized in the atmosphere. The most long-lived sulfur species in the troposphere is carbonyl sulfide, which has an average lifetime of 7 years.[1] Highly accurate CCSD(T)/CBS//MP2/aug-pVDZ calculations on all the low-lying structures of $OCS(H_2O)_{n\ =\ 1\text{–}4}$ reveal that the Gibbs free energy for the stepwise addition of successive water molecules is 2.92 (n = 1), 3.64 (n = 2), −1.25 (n = 3), and 1.35 (n = 4) kcal mol^{-1}.[121] The negative ΔG° of formation for $OCS(H_2O)_3$ from the addition of a third water molecule to $OCS(H_2O)_2$ is a common phenomenon in these types of calculations, as three to five water molecules form planar cyclic structures that lower the overall energetics.[46,52] Given the average concentration of OCS in the atmosphere of 1.23×10^{10} molecules per cm^3, the predicted concentration of $OCS(H_2O)$ is on the order of 10^6, while that of $OCS(H_2O)_2$ is on the order of 10^2.[121] This is another interesting idea: that is, as monomers always have a higher concentration than dimers, and dimers have a higher concentration than trimers, the stepwise energetics must be considered with a known or assumed concentration to predict how large certain clusters will grow in the atmosphere. For water itself, CBS-APNO calculations lead to the prediction of 10^{14} dimers, 10^{12} trimers, 10^{11} tetramers, 10^{10} pentamers, and 10^4 hexamers per cm^3 at S = 1 and 298 K.[122] Overall, our work and the work of others lead to the prediction that most molecular species in the atmosphere will be hydrated to some extent, forming gas-phase atmospheric clusters.

2.2 | Reaction pathways leading to SOL

Organic particulate matter (OPM) represents a significant fraction of the atmospheric aerosol budget and has important implications in climate and public health.[123] Depending on their formation processes, these aerosol particles can be classified as primary organic aerosols, which are emitted directly into the atmosphere from various sources, or SOAs, which are formed from the oxidation (usually by OH radicals) of organic gas-phase compounds and the subsequent condensation into aerosol PM.[124–126] Laboratory studies have shown that the formation of SOAs occurs in a complex system impacted by trace gases in the troposphere, such as NO_X ($NO + NO_2$) and SO_x ($SO + SO_2 + SO_3$). This complexity presents challenges in modeling SOA formation processes, resulting in an oversimplification of SOA sources in atmospheric models and therefore large uncertainties in assessments of the impacts of SOAs on climate and health.

Over the last several years, QM calculations have provided a better molecular understanding of gas-phase reactions leading to SOA formation. Many of these reactions can be described as photo-induced, where atmospheric thermal energy alone is not enough to initiate the chemistry that generates aerosol particles; instead, excited species generated by solar radiation, such as OH radicals, trigger the reactions that ultimately form SOAs.[124,127–129] Other pathways involve reactions between gas-phase organic compounds and trace atmospheric gases, leading to low-volatility products that ultimately form SOAs in the absence of light. In this section, we briefly summarize various reaction pathways that lead to SOA formation modeled using QM methods.

Hydroxyl radicals (OH), generated during daytime from the dissociation of ozone (O_3) and the subsequent reaction of $O(^1D)$ with H_2O,[32,130] are an important oxidizing agent that control aerosol aging and secondary PM. Most daytime reactions of volatile organic compounds (VOCs) that produce functionalized organic products, whose lower volatility and higher solubility allow for SOA formation, involve $^\bullet OH$ and O_3.[123,131,132] Such secondary aging processes also involve other trace atmospheric gases such as NO_X, which increases reaction complexity and affects the formation and optical properties of SOAs. Over the last decade, modeling these daytime reactions has provided important insights into the roles of trace gases in SOA formation mechanisms.

In general, reactions pathways in the troposphere involving OH radicals follow a second-order bimolecular reaction, $^\bullet OH + VOC \xrightarrow{k}$ Products, where k represents the kinetic constant. Recently, QM calculations have been used to model pathways of OH reactions with molecular proxies of VOCs. Computationally generated potential energy surfaces (PESs) provide activation energies of multiple-step photoxidation reactions. These QM calculations allow for the estimation of the reaction kinetic constant ($k(T)$) using the Eyring equation[133,134]

$$k(T) = \sigma \frac{\kappa_B T}{h} \frac{q_{TS}^{\ddagger}}{q_R q_P} e^{-\frac{E_a}{\kappa_B T}} \tag{2}$$

where E_a, κ_B, and h represent the activation energy and the Boltzmann and Planck constants, respectively.The terms $q_{TS}^{\ddagger}$, q_R, and q_P are the total partition functions of the transition state, reactants, and products, respectively. The collision cross-section σ, includes an Eckart tunneling correction.[135] A recent application of this QM method was the use of the ωB97X-D/6-311++G(2df,2pd) model by Milhøj et al to compute the activation barriers of the reaction between adenine and OH radical.[136] Their E_a calculations led to the resulting overall rate constant for the reaction at

298 K, $k = 2.17 \times 10^{-12}$ cm^3 per molecule per second, a significant improvement over previous estimates. Similarly, Chu et al determined pathways of •OH reactions with acrylic acid, an unsaturated carboxylic acid and model system for VOCs in the atmosphere.[137] The models show a five-step process leading to the oxidation of acrylic acid via hydrogen abstraction and C addition. PESs of this reaction were calculated via geometry optimizations of reactants, intermediates, and activated complexes by BH and HLYP and M06-2X functionals, with a 6-311++G(d,p) basis set. Calculated activation energies allowed for the estimation of the kinetic constant using Equation (2).[136,138] Chu et al determined that k_{OH}(200 K) = 2.3×10^{-11} cm^3 per molecule per second for the pseudo-first-order reaction, assuming a constant global atmospheric concentration of OH radical (2.0×10^6 molecules per cm^3). This calculation provided an estimated atmospheric lifetime of acrylic acid of approximately 20 minutes, calculated using $\tau = (k_{OH}[OH])^{-1}$,[139] which is in good agreement with experimental data (~22 minutes).

Similar PESs were calculated recently for the aqueous-phase reaction of catechols and nitronium ions (NO_2^+) to model the effects of NO_X on the atmospheric aging of VOCs and the formation of nitrated SOAs.[140] Nitroaromatic compounds present in SOAs are especially important catechol derivatives known to have significant impacts on climate and health.[141,142] Because nitrocatechols are formed in the presence of NO_X, understanding the mechanisms that lead to their formation provides a molecular-level understanding of the effects of anthropogenic activity on the atmosphere. Frka et al investigated the formation of methylnitrocatechol using the ab initio method MP2/6-31++G(d,p). While B3LYP density functional gave results comparable to those obtained via the MP2 level of theory used in this work, B3LYP failed in computing local minima for aromatic nitration pathways.[143] 3-Methylcatechol was used as a model system for the nitration reaction with NO_2^+. The theoretical calculations suggest three possible reaction pathways leading to three possible products, 3-methyl-4-nitrocatechol (3M4NC), 3-methyl-5-nitrocatechol (3M5NC), and 3-methyl-6-nitrocatechol (3M6NC), as shown in Figure 2 (left). The same calculations show that nitration on site 6 not only is thermodynamically unfavorable but also has the largest activation barrier (dashed red line in Figure 2, right), in agreement with previous work by Andino et al.[144] Thus, QM results show that nitration at sites 4 and 5 is favored with negligible nitration at site 6, which is consistent with field and experimental measurements.[140]

Similar to the work by Chu et al, this activation barrier calculation allowed for determination of the kinetic constant of catechol nitration using Equation (2), with the kinetic constants (k) at 298 K of 1.1×10^{10}, 2.6×10^{10}, and 1.4×10^4 s^{-1}, for 3M4NC, 3M5NC, and 3M6NC, respectively. As anticipated by the difference in activation energies shown in Figure 2 (right), the reaction rate constants are six orders of magnitude larger for nitration at sites 4 and 5 than that at site 6, which further proves the higher favorability of reaction at sites 4 and 5 and indicates an electrophilic pathway for the reaction shown in Figure 2 (left).[140]

Similar pathways for the oxidation of isoprene, the most abundant non-methane hydrocarbon emitted into Earth's atmosphere, by OH radical provide an important daytime source of SOAs in the troposphere.[124,145–147] This process is important to the balance of hydrogen oxide (HO_X = HO + HO_2) radicals over vegetated areas and impacts ozone levels in urban areas.[145] Recently, experimental work and modeling simulations have suggested that SOA formation from the photoxidation of isoprene is enhanced by anthropogenic pollutants such as NO_X and SO_2.[145,147] Isoprene oxidation occurs by way of hydroxyl peroxy (RO_2) radical formation, and the fate of these radicals is dependent on the concentration of nitrogen oxides (NO_X = NO_2 + NO).[145] Under low-NO_X conditions, RO_2 radicals react mostly with HO_2 to form lower volatility oxidation products and, in turn, relatively high yields of SOAs. In contrast, under high-NO_X conditions, RO_2 radicals tend to react with NO, producing alkoxy (RO) radicals that are likely to fragment into smaller, more volatile products, thus resulting in lower SOA yields.[145] DFT calculations carried

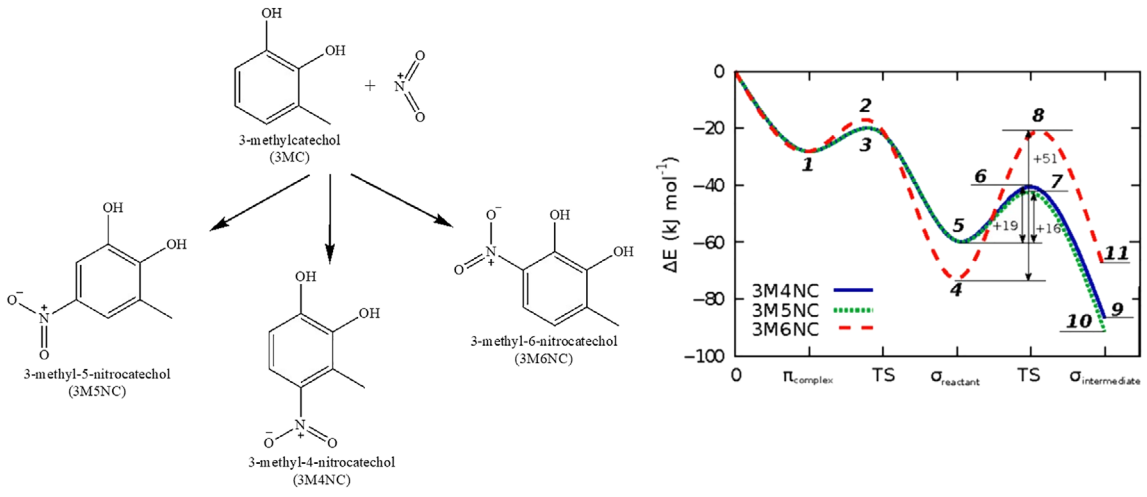

FIGURE 2 Left: reaction scheme for the nitration of 3-methylcatechol in aqueous phase. Right: PES for the reaction of 3-methylcatechol (3MC) with nitronium ions (NO_2^+). Three different reaction pathways lead to the formation of 3-methyl-4-nitrocatechol (3M4NC), 3-methyl-5-nitrocatechol (3M5NC), and 3-methyl-6-nitrocatechol (3M6NC). The labels in the PES indicate the number of structures (intermediates, activated complexes, and products) optimized by Frka et al[140]

out by Lin et al verified the NO_X influence over SOA formation.[146] Quantum chemistry, at the m062× density functional and 6-311++G(d,p) basis set, was used to calculate the relative zero-point energy (ZPE) and product yields for the reaction involving intermediate methacryloylperoxynitrate (MPAN) and •OH.[146] These calculations, combined with experimental data, suggest that the chemical pathway for SOA formation from isoprene in the presence of NO_X involves nitration of oxidized isoprene and a gas-phase intramolecular rearrangement, yielding nitrate and methacrylic acid epoxide (MAE) as products. The overall process is shown in Scheme 1. The formation of SOAs results from the lower volatility and higher solubility of MAE under acidic atmospheric pH.

Energy minimizations and vibrational frequency calculations were used to determine the chemical kinetics parameters, including the total rate constant and yield of the reaction leading to the formation of MAE. The main reaction pathway for MAE formation is the addition of OH radical to the nitrated intermediate MPAN.[146]Under low-NO_X conditions, isoprene epoxidiols (IEPOX = β-IEPOX + δ-IEPOX) form as intermediates rather than MPAN.[145] In this case, the presence of acidified sulfate seed enhances SOA formation over that in the presence of neutral aerosols due to increased uptake of IEPOX by acid-catalyzed particle-phase reactions. Laboratory chamber studies performed by Surratt et al showed the enhancement of isoprene SOA yields by a factor of 22 with increased aerosol acidity.[145] Under high-NO_X conditions, the aerosol phase becomes acidic enough to facilitate high SOA yields in the presence of nitric acid (HNO_3) and/or organic acids.[145] Additional work on the aging of other terpenes, an important class of VOCs made from isoprene monomers, has shown that the oxidation of VOCs is spontaneous once initiated by trace gases such as O_3 and that the reaction accelerates in the presence of water.[148]

In the past two decades, substantial work has been done on low-volatility species, which are of crucial importance to SOA formation. Chamber studies quantifying SOA yields from VOC oxidation often report measurements below observed SOA concentrations in field studies. Kroll et al justified this disparity as evidence of additional pathways of SOA formation from low-volatility parent compounds, primarily semi-volatile organics, which are present in both gas and particle phases and allow SOA formation to be characterized by gas-particle (G/P) partitioning theory.[124] However, Tong et al argued that G/P partitioning theory, while largely suggesting previously unrecognized pathways in SOA formation and dynamics, underestimates SOA concentrations because it excludes volatile products such as aldehydes and ketones. These products are absorbed into the aerosol phase, where they undergo heterogeneous aerosol-phase reactions with low-volatility products that ultimately increase OPM.[149]

To thermodynamically evaluate these reactions, Tong et al developed a computational method for the QM calculation of ΔH_f^0, ΔS^0, and ΔG_s^0 (solvation energy) for a given species. Heats of formation were calculated from ground-state energies obtained via gas-phase geometry optimizations at the DFT/X3LYP level of theory with the basis set aug-cc-pVTZ(−f), and from ZPEs as well as vibrational, rotational, and translational

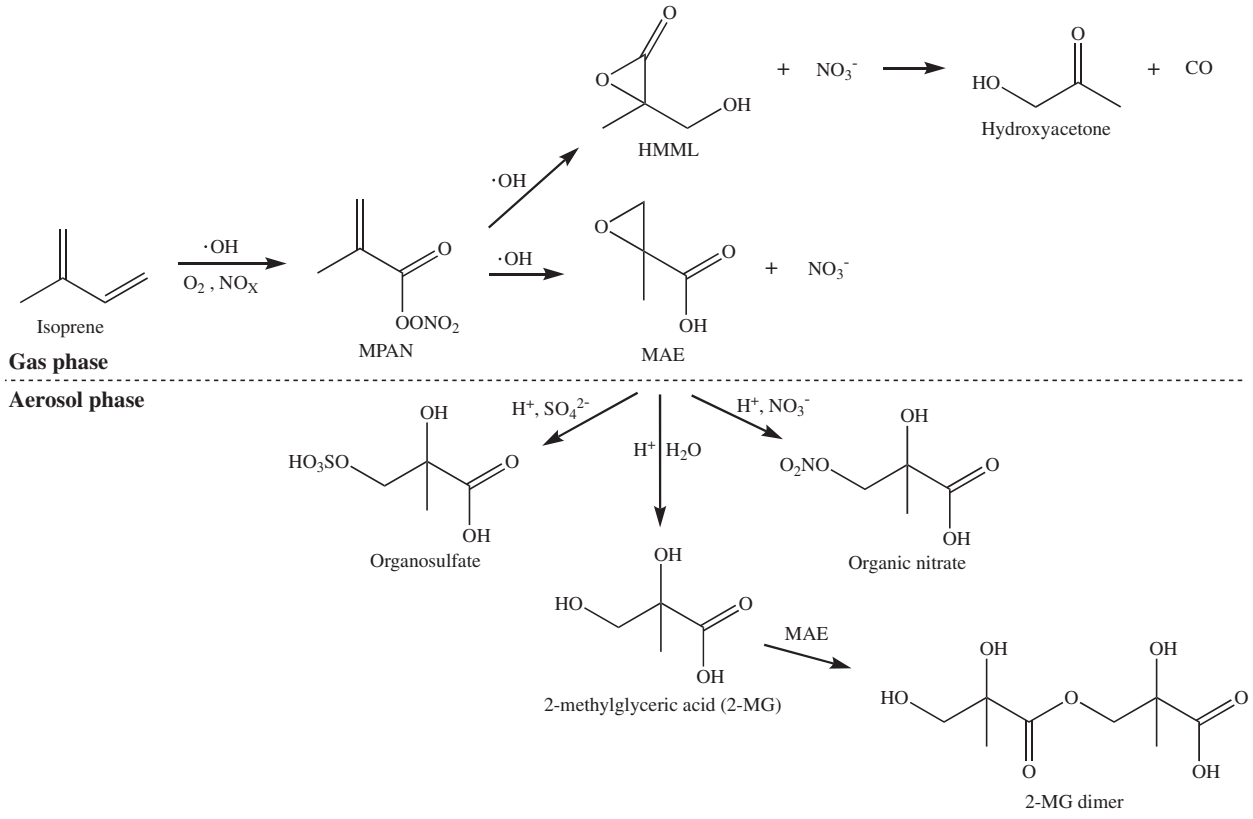

SCHEME 1 Mechanism based on the work by Lin et al for SOA formation from isoprene photoxidation in the presence of NO_2[146]

enthalpies obtained via vibrational frequency calculations at HF 6-31G(d,p). A correction scheme, such as the J2 model based on the GVB-LMP2 method, was recommended to account for discrepancies between QM and experimental results. In solution phase, reoptimization at X3LYP/cc-pVTZ(−f) using the implicit continuum solvent model accounted for changes in entropy due to conformational changes.[149]

Similar methods were used by DePalma et al in a study of oligomer formation, which occurs via the linkage of two or more monomeric VOC oxidation products.[150] The authors argued that the deficiency of G/P partitioning theory in quantifying SOA lies in its failure to account for oligomerization. The complexity of oligomer formation, which can result in over a thousand unique products from the oxidation of a single parent VOC, requires the coupling of experimental and theoretical techniques for an accurate gauge of oligomer impacts on SOA formation. Functional groups of monomers involved in oligomerization include alcohols, carboxylic acids, ketones, aldehydes, and peroxides, which undergo dimerization reactions such as aldol addition, esterification, and anhydride formation. The calculations of DePalma et al involved multicomponent clusters aimed to provide a deeper understanding of the properties of aerosols with complex composition formed from the ozonolysis of α-pinene. DFT and continuum solvent modeling were combined with MC sampling and semiempirical QM to determine thermodynamically favorable oligomer formation pathways. All geometry optimizations used the AM1 level of theory. The field energy of each structure was sampled via MC conformational sampling, and vibrational frequencies were calculated using PW91/6-31++G(d,p). Both gas- and condensed-phase dimerization free energies were calculated as single-point energies using the PW91 functional with basis sets 6-311++G(2d,2p) and 6-311++G(3df,3dp); the appropriate geometric and thermal corrections were determined from the basis set PW91/6-31+G(d,p) and were scaled by 0.982. Solvation effects for condensed-phase compounds were accounted for by the calculation of ΔG_s using the SMD universal continuum model and by post-solvation reoptimization. In general, favorable gas-phase dimerization processes were found in noncovalent dimers of VOC models terpenylic acid and/or *cis*-pinic acid, and covalently bound peroxyhemiacetal. Several noncovalent dimers, such as the peroxyhemiacetal dimer and the homodimers of *cis*-pinic acid and terpenylic acid, were also found to be favorably formed in the condensed phase. However, only terpenylic acid was found to dimerize and contribute to new SOA formation under atmospherically relevant conditions. The fraction of dimers to monomers was often found to exceed 10%, a ratio large enough to impact overall SOA formation processes. The computationally obtained results of this study were in agreement with recent experimental findings.

In a recent QM calculation seeking to model the formation and growth of atmospheric particles with a complex composition, Xu et al used small clusters of atmospherically relevant acid/base VOCs. Proton transfer properties of methanesulfonic acid (CH_3SO_3H), methylamine (CH_3NH_2), oxalic acid ($C_2H_2O_4$), and water were studied using QM simulations and were correlated with experimental observations on new particle formation.[151] All geometry optimizations were carried out using the B3LYP functional with Grimme's dispersion correction and Dunning's augmented double-ξ correlation-consistent basis set aug-cc-pVDZ. These levels of theory, along with MP2 calculations, were found to yield ΔG values comparable to the experimental ones.[151,152] All complexes minimized the examined proton transfer between the conjugate acid and conjugate bases. Figure 3 shows two of the most stable binary complexes, namely $[CH_3SO_3]^-$:$[CH_3NH_3]^+$ and $[C_2HO_4]^-$:$[CH_3NH_3]^+$.

The binary structure simulating the proton transfer between the acid CH_3SO_3H and the base CH_3NH_2 (Figure 3A) shows the highest proton transfer (δ = 0.83), in agreement with the strong acidity of CH_3SO_3H (p*K*a = −1.9).[151,153] When the binary complex used the weak acid $C_2H_2O_4$ (pKa_1 = 1.3 and pKa_2 = 3.6),[154] shown in Figure 3B, the complex was driven by hydrogen-bonding interactions, resulting in the lowest proton transfer (δ = 0.13). As tertiary and quaternary complexes were examined, proton transfer took place in all cases involving the strong acid CH_3SO_3H. The calculated proton transfer of the acid–base small cluster system correlates well with the experimentally found ability of the system to form new particles. Significant particle concentrations were found in experimental studies when a high proton transfer was calculated. In general, QM calculations are providing substantial molecular-level studies on pathways for SOA formation and growth of new particles in the atmosphere, with DFT calculations proving accurate to predict VOC atmospheric lifetimes and SOA yields in urban and rural environments.

3 | SURFACE CHEMISTRY AND PHOTOCHEMISTRY THROUGH QUANTUM CHEMISTRY

Atmospheric aerosols, both primary and secondary, are known to provide active surface sites for the adsorption of trace atmospheric gases.[18] Depending on the strength of the substrate–surface interactions, the adsorption process can be classified as physisorption, driven by van der

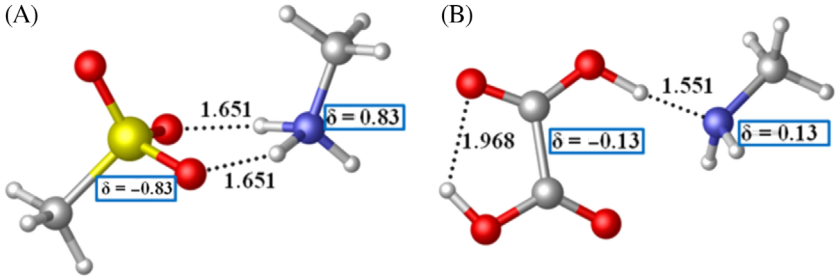

FIGURE 3 Geometry optimization at the B3LYP-D3/aug-cc-pVDZ level of theory of the most stable binary complexes: A, $[CH_3SO_3]^-$:$[CH_3NH_3]^+$ and B, $[C_2HO_4]^-$:$[CH_3NH_3]^+$. Partial charges (δ) are reported in atomic units and interatomic distances in angstroms[151]

Waals forces, or chemisorption, with covalent-like interactions. Atmospheric trace gases adsorbed onto a particle surface undergo symmetry-breaking processes in which geometry perturbations change the optical properties and the HOMO–LUMO gaps of the surface species.[32] These changes open heterogeneous reaction pathways that cannot take place in a homogeneous system. Understanding the structural distortions resulting from the gas–particle interaction is, therefore, paramount to our understanding of aerosol impacts on the atmospheric chemical balance and energy budget.

QM computational methods have been implemented to model spectroscopic data of chemisorbed and physisorbed species on several components of mineral dust, combustion particles, and sea-spray aerosols. Such models have increased our understanding of not only the adsorption mechanism of trace atmospheric gases but also surface-mediated reactions. Simulations of surface processes on metal oxides, which serve as proxies for mineral dust or combustion particles, are usually carried out using a two-metal-atom cluster to represent the substrate's active site. The cluster is usually modeled based on existing crystal structure information, where the geometry of the substrate is not minimized. Hydrogen terminals are typically included to maintain the cluster's neutrality at a singlet ground state. This approach does not model the bulk properties of the atmospheric particle but allows for calculations of surface processes of the system at a lower computational cost. Other approaches include the optimization of a multiple-atomic-layer slab of a metal oxide with one unit cell used for all calculations. Here we summarize the interaction of trace atmospheric gases with model systems of mineral dust or combustion particles. In particular, we discuss conformational energies and spectroscopic simulation of adsorbed nitrates (NO_3^-), carbon dioxide (CO_2), and sulfur dioxide (SO_2), as well as the effects of coadsorbed water.

3.1 | Surface-bound nitrates and nitric acid

Nitric acid (HNO_3) is a natural trace gas that forms from reactions of NO_X with atmospheric water. Gaseous nitric acid reaches higher concentrations in the troposphere near populated areas as a result of higher NO_X emissions and photochemical smog.[155] Until recently, nitric acid was considered to be a natural atmospheric nitrogen sink. However, experiments involving irradiation of broadband light onto nitric acid adsorbed on alumina (Al_2O_3), a common component of mineral dust and combustion particles, showed a surface-mediated photochemical mechanism that produced HONO, N_2O, and NO_X; this renoxification reaction likely occurs in the troposphere and is triggered by aerosol particles and solar radiation.[25,26,156] In order to examine this reaction at a molecular level, Baltrusaitis et al performed DFT calculations of ground-state vibrational frequencies of nitrate adsorbed onto Al_2O_3, matching the experimental vibrational spectra with calculated frequencies adjusted for anharmonicity.[157] Geometry optimizations of chemisorbed nitrates were carried out using a binuclear cluster $([Al_2O_3\,(OH)_n(H_2O)_2(NO_3)]^{-1}$ where n = 4 or 5) with the basis set B3LYP/6-31 + G(d), which was found to be suitable for geometry optimization. Vibrational frequency calculations were also performed at the B3LYP/6-31 + G(d) level of theory. The calculations showed that nitrate geometry is altered upon adsorption, changing from the C_{2V} point group for "free nitrate" geometry to D_{2h} for adsorbed nitrate. In addition, nitrate was shown to chemisorb onto Al_2O_3 following three binging geometries, as shown in Figure 4.

Compared to the C_{2V} structure, the less symmetric D_{2h} is more reactive in the presence of solar radiation, which is consistent with the aforementioned heterogeneous photochemical pathway of adsorbed nitrates. Recently, Ostaszewski et al carried out QM calculations to simulate the vibrational spectra of nitric acid chemisorbed on TiO_2, a semiconductor component of mineral dust and combustion particles with a bandgap of 403 nm,[32,158–160] which corresponds to an energy value below the atmospheric cutoff of solar radiation.[21] Similar to the calculations done on Al_2O_3, the geometry optimization and the vibrational frequencies were calculated using the B3LYP/6-31 + G(d) level of theory, adjusted for anharmonicity factors.[157] While the same symmetry-breaking phenomenon was observed on nitrates adsorbed on both TiO_2 and Al_2O_3, only two variations of chelating complexes were observed on TiO_2, due in large part to the lattice dimensions that prevented the bidentate nitrate structure from forming. Ostaszewski et al reported six different surface nitrate geometries, all variations of monodentate or bidentate structures as shown in Figure 4A. Overall, this work shows that surface-mediated photochemistry on semiconductor components results from a combination of electron–hole pairs reacting with surface nitrates and D_{2h} nitrates reacting in the presence of light.[21]

3.2 | Surface-bound carbon dioxide, carbonates, and bicarbonates

Another important trace gas with significant climate implications is CO_2, the fourth most abundant gas in the atmosphere.[20] Recently, studies on heterogeneous CO_2 reactions with atmospheric PM examined the adsorption of gaseous CO_2 onto the faujasite zeolites NaY and BaY, which are

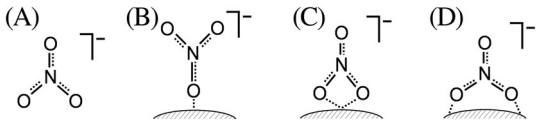

FIGURE 4 Schematic diagram of "free nitrates" (C_{2V} point group), surface nitrates, and adsorbed nitrates (D_{2h} point group). A, Nitrate; B, monodentate; C, bidentate; D, bridging

cation-stabilized aluminosilicate materials.[20] Galhotra et al conducted DFT calculations at the B3LYP LanL2DZ level of theory to understand the vibrational frequencies of adsorbed carbon dioxide, along with surface-bound reaction products carbonate and bicarbonate. For carbonate and bicarbonate models, geometry optimizations were carried out on the neutral clusters $BaCO_3$, Na_2CO_3, $BaOH(CO_3H)$, and $Na(CO_3H)$.[20] These calculations indicated that symmetry-breaking follows the adsorption of CO_2 onto a modeled neutral zeolite structure; this symmetry-breaking led to IR activation of the ν_1 vibrational mode due to a strong surface influence. Additionally, the asymmetry of the adsorbed CO_2 caused the ν_2 bending mode to separate into two modes: in-plane and out-of-plane. The matching of calculated vibrational frequencies of adsorbed carbonates and bicarbonates onto the faujasite zeolites confirmed a surface-mediated reaction. Similar to the ν_2 bending mode in carbon dioxide, carbonates and bicarbonates underwent a separation of the ν_3 bending mode into two vibrational bands. DFT calculations were in agreement with those found experimentally under both dry and humid conditions (vide infra).

Other QM studies of CO_2 interaction with atmospheric aerosol components include studies on adsorption onto titania (TiO_2), an important semiconductor component of PM.[32] The work of Indrakanti et al examined computationally the chemisorption of ground-state carbon dioxide onto titania polymorph anatase (001), (101), and (010) surface planes.[161] Titania serves as an important catalyst for the photoreduction of CO_2, with anatase having the highest catalytic activity; this photoreduction pathway could prove useful to technological developments in intermittent solar energy and the reduction of fossil fuel consumption.[159] Similar to Galhotra's work, Indrakanti et al used DFT frequency calculations to understand the convoluted vibrational spectra of CO_2 adsorbed on TiO_2.[161] The optimized geometries were calculated at the B3LYP/6-31+G (d) level of theory using the neutral binuclear cluster $Ti_2O_9H_{10}CO_2$. Calculated vibrational frequencies for all three surface planes were consistent with experimental observations. Each of the three surfaces showed a distinct configuration of vibrational bands corresponding to carbonate-like species adsorbed on the surface. Furthermore, the adsorption of CO_2 results in an O–C–O angle distortion with a slight negative charge ranging from −0.3 to −0.45 e^-, suggesting a partial reduction of CO_2. Through the localized ground-state cluster approach, Indrakanti et al modeled the adsorption process of CO_2 onto titania anatase surfaces, which furthered our understanding of reactive species created on metal oxide surfaces.

3.3 | Surface-bound sulfur dioxide

Sulfur dioxide (SO_2), a precursor of sulfuric acid (H_2SO_4), is emitted into the atmosphere via natural processes (volcanic activity) and anthropogenic activity (combustion of oils and coal).[162–167] As was mentioned in Section 2.1, sulfuric acid molecules are hygroscopic and can serve as cloud condensation nuclei.[162,163,168] Thus, a greater understanding of atmospheric SO_2 behavior yields better climate modeling and insights into human and environmental health. Recent work has investigated the adsorption of SO_2 onto mineral aerosols, which may act as a sink for sulfur dioxide and other trace atmospheric gases.[168,169] Zhao et al examined the adsorption of SO_2 onto hematite (α-Fe_2O_3) under dry aerobic conditions via PBE-GGA for the exchange correlation functional paired with the Hubbard model U interaction.[168] Figure 5 shows the five stable SO_2

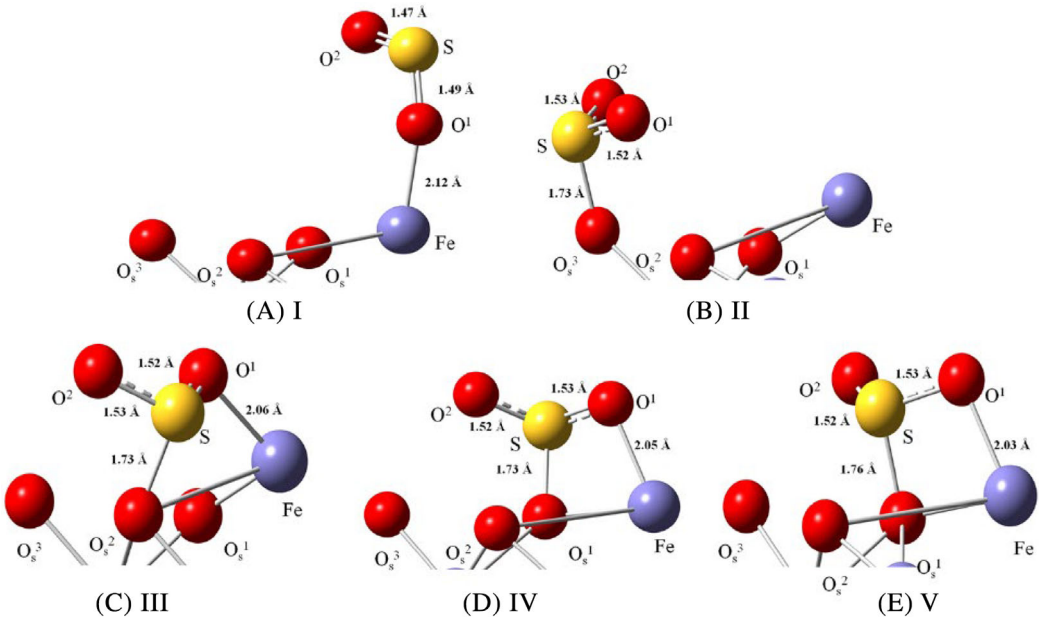

FIGURE 5 The five (A–E) stable structures of SO_2 adsorbed on the α-Fe_2O_3 surface as calculated by Zhao et al.[168] Structure I is unfavorable and structures II–V are favorable, with structure V being the most stable

adsorbed structures found by Zhao et al to exist on α-Fe_2O_3. Four of the structures exhibited strong SO_2–surface interactions through the distortion of the calculated O–S–O bond angle from 119° to 108°–109°, indicating those structures to be the most favorable.

Elongation of S–O bonds from the gas phase to the adsorbed phase suggested that the adsorbed species resembled SO_3. This was supported by the calculated vibrational frequencies—of the three vibrational modes of gas-phase SO_2, the antisymmetric stretching mode ν_{as} underwent a red shift of 308–313 cm^{-1}, suggesting a lengthening of the S–O bonds. Additionally, the calculated adsorption energies ranging from −0.97 to −0.83 eV demonstrated the stability of the SO_3-like adsorbed species in the four most stable structures shown in Figure 5. The significant charge transfer between the adsorbed SO_2 and the hematite surface in the most stable structure is indicative of chemisorption. The least stable structure (structure I) showed a decrease in charge transfer, suggesting physisorption, and entropic effects indicated low coverage of the hematite surface, even at SO_2 pressure as high as 1 atm. Under aerobic conditions, Zhao et al found the adsorption of the only stable geometry of O_2 on the hematite surface to be weak, with an adsorption energy of −0.31 eV, compared to the −0.97 eV adsorption energy of the most stable SO_2 interaction with hematite. SO_2 was therefore preferentially adsorbed on the hematite surface, and O_2–SO_2 interactions were found to take place on the surface and yield sulfate and bisulfate products. Compared to the sum of these two gases' individual adsorption energies, −1.28 eV, the energies of the SO_4 species' adsorption onto the hematite surface were larger, ranging from −1.31 to −1.65 eV. Thus, SO_4 adsorption was favored over the individual adsorptions of SO_2 and O_2. Entropic effects supported the favored adsorption of SO_4, and vibrational frequencies indicated that three of the four stable geometries were bidentate structures, while one was a tridentate structure.

In a similar study, Lo et al investigated the chemisorption and physisorption of SO_2 on γ-Al_2O_3, for both a clean (100)E surface and a dehydrated (110)C surface. All computational calculations were run through the Vienna ab initio simulation package (VASP). Geometry optimization employed the conjugate-gradient algorithm—vibrational frequency calculations used the harmonic approximation and double finite differences method; thermodynamic energy profiles were determined via ciNEB and RMM-DIIS methods.[162] Results indicated that physisorption took place on the γ-Al_2O_3(100) surface when SO_2 adsorbed onto a μ_3-O atom, and chemisorption took place when SO_2 adsorbed onto a terminal O atom. For both the clean (100)E surface and the dehydrated (110)C surface, the most stable configurations were tridentates and bidentates, which is in agreement with the conclusions drawn by Zhao et al.[168] In Lo et al's study, stabilities were determined by the energy profiles, in which the most stable configuration on the clean (100)E surface had an energy of −45.24 kcal mol^{-1}, and the most stable configuration on the dehydrated (110)C surface had an energy of −70.82 kcal mol^{-1}.[162] Thus, adsorption of SO_2 to the γ-Al_2O_3 surface was found to be favorable. Calculated IR vibrational frequencies were supported by experimental data.

3.4 | The effects of coadsorbed water through quantum chemistry

Water coadsorbed onto a surface has been studied in concert with the adsorption of the trace gases CO_2, NO_2, and SO_2. In general, surface water plays a dual role in the chemistry that takes place on the surface of atmospheric particles. First, water competes for active surface sites, preventing the adsorption of trace atmospheric gases. Second, adsorbed water undergoes surface-promoted reactions similar to those described for trace gases. For instance, water on TiO_2-anatase undergoes an apparent dissociative adsorption in which a proton transfers to the oxygen bridging Ti centers in the TiO_2 crystal structure.[170–172] This dissociation ultimately leads to an increase in OH surface density, with consequential effects on the adsorption of atmospheric gases, water uptake, and cloud formation.[13,14,173–176]

Baltrusaitis et al conducted a study on the effect of coadsorbed water on the adsorption of carbon dioxide onto metal oxides using the B3LYP/6-31G(d) level of theory.[177] Under dry conditions, bicarbonate groups were the major product from the reaction of surface hydroxyl groups with adsorbed CO_2; wet conditions led to the formation carbonic acid, which was deprotonated to yield adsorbed carbonate and protonated hydroxyl groups such as Fe-OH_2^+. These findings were supported by a mononuclear cluster system of $[Al(OH)_3(H_2O)_n(CO_3)]^{2-}$ where n = 0–4. With increased solvation, bond length changes showed that the geometry of the carbonate ion was less distorted, and a decrease in the difference between the ν_3 vibrational modes indicated that the carbonate ion was relaxing to a less coordinated state. Similar findings were made by Galhotra et al in a study on the effect of coadsorbed water on interactions between CO_2 and zeolite surfaces using the B3LYP LanL2DZ level of theory.[20] Results showed that coadsorbed water on the zeolite surface, especially with the barium cation BaY, decreased the number of active sites available to adsorb CO_2 and therefore led to a decrease in the magnitude of ν_3 band splitting from 615 cm^{-1} under dry conditions to 506 cm^{-1} in the presence of two solvated water molecules. This decrease shows the same relaxation to a less coordinated state found in Baltrusaitis' work.[20,177]

Baltrusaitis et al also conducted a study on the adsorption of nitrate onto aluminum oxide surfaces in the presence of coadsorbed water using a binuclear $[Al_2(OH)_3(\mu\text{-}OH)_2(H_2O)_{11}(NO_3)]$ cluster analyzed at the B3LYP/6-31 + G(d) level of theory.[178] While dry conditions yielded monodentate, bidentate, and bridging clusters, full solvation conditions at high RH yielded complexes in which nitrate was directly bound to the binuclear alumina cluster, as well as complexes in which nitrate was not directly bound. Bond lengths, geometries, and vibrational frequencies for both high-RH complexes were calculated and were in agreement with experimental data. Another study by Ostaszewski et al examined the ground states of nitrate adsorbed onto TiO_2 with coadsorbed water using a $[Ti_2O(OH)_n(H_2O)_2(NO_3)]^{-1}$ cluster where n = 4 or 5, at the B3LYP/6-31 + G(d) level of theory.[21] This work found modes similar to those reported by Baltrusaitis et al, but as the number of water molecules present

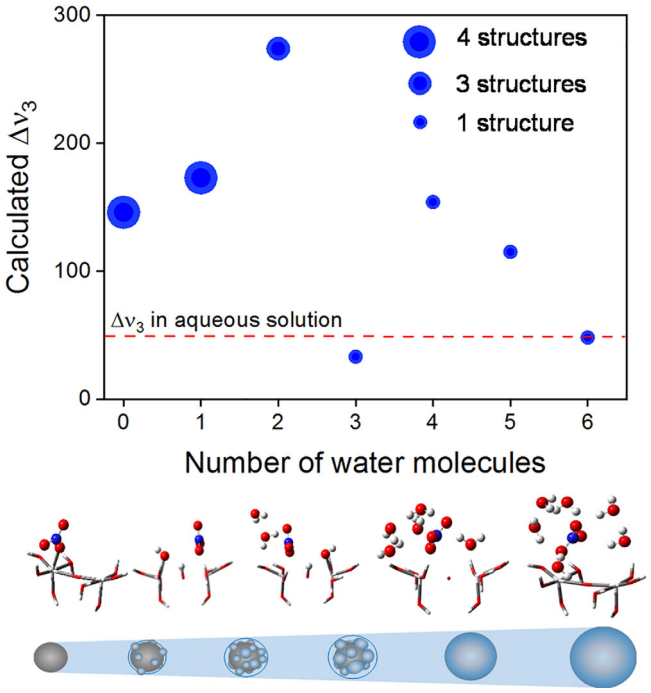

FIGURE 6 Top: Effect of coadsorbed water on surface nitrate structures and vibrational frequencies. Size of the symbols represents the number of surface-bound nitrate geometries minimized and matches with experimental data. The split ν_3 vibrational features show three regimes: first, from dry to two water molecules, several nitrate structures exist on the surface and the ν_3 vibrational features diverge to nearly 300 cm^{-1}; second, for three water molecules, the nitrate coordination number on the TiO_2 surface decreases to only one structure (monodentate), which shows a close interaction with the surface and a highly symmetric structure approaching D_{3h} symmetry. Finally, as more water molecules are added to the model, the two ν_3 vibrational features initially separate more, only to converge towards the vibrational frequencies expected for aqueous-phase nitrate ($\Delta\nu_3$ = 49 cm^{-1}). Bottom: Monodentate TiO_2-nitrate representation

increased from 0 to 6, competition for active sites between water and nitrate occurred, hydrogen-bonding interactions increased, and symmetry-breaking of adsorbed nitrate decreased. Beyond three water molecules in the cluster, only the monodentate mode of nitrate was possible, resulting in a single geometry coordination. Ostaszewski et al showed that upon adsorption of water, the vibrational frequencies of adsorbed nitrate resembled those of aqueous-phase nitrate, as the two ν_3 vibrational features initially separated by the surface effect converged towards the vibrational frequencies expected for aqueous-phase nitrate, shown in Figure 6 as a decrease in the ν_3 split ($\Delta\nu_3$).[21] These simulations also showed that coadsorbed water limited the degrees of freedom of adsorbed nitrate, decreasing the number of structures as more water was added to the cluster. Once three water molecules were added to the simulation, only a monodentate structure was minimized, approaching the C_{3V} point group as evidence in the low $\Delta\nu_3$. These computations were in agreement with experimental data, which showed less convoluted vibrational spectra at higher RH levels.

Both Zhao et al and Lo et al conducted computational studies on the effects of wet conditions on SO_2 adsorption onto metal oxide surfaces via their aforementioned respective methods.[162,168] Zhao et al first determined that when a clean hematite (0001) surface was exposed to water molecules, water dissociated, resulting in hydroxylated hematite. This finding was supported by changes in bond lengths and by the dissociation energy being 0.25 eV lower than the adsorption energy. Thus, SO_2 was coadsorbing with hydroxyl groups rather than with water. The same study found that with an adsorption energy of −0.50 eV, SO_2 was physisorbed onto a surface hydroxyl group. However, at typical atmospheric SO_2 concentrations, the entropic gains of SO_2 in gas form were found to surpass the adsorption energy, indicating that adsorption of SO_2 to the hydroxylated surface was unfavorable. Calculated bond lengths of the adsorbed species, which were similar to those of a free SO_2 molecule, were in agreement with this thermodynamic conclusion. RH therefore has little effect on SO_2 adsorption. Similarly, Lo et al's study reported two modes in which SO_2 was physisorbed onto a surface hydroxyl group of a hydrated γ-Al_2O_3(110) surface with extensive hydrogen bonding.[162] Three other modes were found that produced adsorbed bisulfite and sulfite. Adsorption enthalpies ranged from 17.53 to 34.79 kcal mol^{-1}, and the most favorable mode was that which formed sulfite. From these results, it was found that SO_2 showed no selectivity between the clean (100)E surface and the hydrated (110)C surface.

4 | CONCLUSIONS AND IMPACT

The complexity of aerosol particles has led to significant gaps in knowledge of the chemistry that controls the processes that drive atmospheric PM. Therefore, there are large uncertainties in the role of aerosol particles in climate and health. Over recent decades, increasing computing power and progress in our understanding of quantum mechanics as pertaining to chemical processes have made computational quantum chemistry a powerful tool to advance our knowledge of atmospheric chemistry. In particular, QM calculations have made significant progress in our understanding at a molecular level of the prenucleation and formation of aerosols. Surface phenomena also increasingly rely on QM calculations, particularly with regard to adsorption processes and conformational energies.

The synergy between experimental methods and computational quantum chemistry has significantly augmented our knowledge of the chemical processes that govern atmospheric particles. Notably, spectroscopic simulation of surface-adsorbed species has advanced our understanding of surface coverages and the relevance of terminal groups regarding heterogeneous chemistry and cloud formation. Quantum chemistry calculations have closed gaps in our knowledge of aerosol formation pathways whose complexity cannot be fully understood through experimental techniques alone. Accurate calculation of transition states has allowed for direct comparison of QM calculations with experimental data and for estimates of atmospheric lifetimes of trace gases. The calculation of PESs has provided a picture of reaction mechanisms and guided experiments. QM calculations applied to atmospheric aerosol represent a unique and reliable method to answer pressing challenges in atmospheric aerosol chemistry:

1. The variable pH between nascent and aged aerosol can affect SOA formation pathways—modeling p*Ka* of carboxylic acids and their effects on reaction pathways is paramount in our understanding of the roles of nascent vs aged aerosol.
2. The optical properties of aerosols and dissolved organic matter and their dependence on pH are still poorly understood. Recent QM calculations have shown that the behaviors of chromophores in the marine environment can open previously unrecognized photosensitization reactions.[179]
3. Since thermal energy alone is not enough to justify all the chemistry taking place in the troposphere and the stratosphere, photochemistry must be simulated.[32] Simulated photochemistry allows for changes in the reactivity of chromophores depending on their excited state. For instance, QM calculations of processes involving excited-state reaction pathways of surface-bound species are needed to understand heterogeneous reactions.
4. Photosensitization mechanisms at different pH levels (combination of challenges 1 and 2) can potentially open additional pathways for SOA formation.

The resolution of the challenges above represents just an excerpt of the potential impact that quantum chemistry computation can have in the near future. As quantum mechanics advances, it is also becoming a common tool used in the classroom at the undergraduate level. Examples that illustrate the application of quantum mechanics to atmospheric phenomena are inspiring a new generation of chemists to study and embark on quantum chemistry. As undergraduate students become more involved in QM calculations, the challenges above will be tackled in new and creative ways. Overall, quantum-based computational strategies provide useful tools to teach chemistry at the undergraduate level and to contribute significant physicochemical insights into atmospheric science.

ACKNOWLEDGMENTS

This work was supported by National Science Foundation grants CHE-1229354, CHE-1662030, CHE-1721511, CHE-1903871 (GCS), NSF Center for Aerosol Impacts on Chemistry of the Environment (CAICE), CHE-1801971, and DBI-1828508 (JGN), the Arnold and Mabel Beckman Foundation Beckman Scholar Award (AGG), the Barry M. Goldwater Scholarship (AGG), and the Schupf Scholar Program (AL). High-performance computing resources of the MERCURY Consortium (http://www.mercuryconsortium.org) were used.[180,181] Authors are grateful for the sea-spray micrograph image from the Vicki H. Grassian group at University of California-San Diego.

AUTHOR CONTRIBUTIONS

Angelina Leonardi: Investigation; writing-original draft; writing-review and editing. **Heather M. Ricker:** Investigation; writing-original draft; writing-review and editing. **Ariel G. Gale:** Writing-original draft; writing-review and editing. **Benjamin T. Ball:** Writing-original draft; writing-review and editing. **Tuguldur T. Odbadrakh:** Writing-original draft; writing-review and editing. **George C. Shields:** Validation; writing-original draft; writing-review and editing. **Juan G. Navea:** Formal analysis; funding acquisition; investigation; resources; validation; visualization; writing-original draft; writing-review and editing.

ORCID

George C. Shields https://orcid.org/0000-0003-1287-8585
Juan G. Navea https://orcid.org/0000-0002-7723-6033

REFERENCES

[1] J. H. Seinfeld, S. N. Pandis, *Atmospheric Chemistry and Physics: From Air Pollution to Climate Change*, 3rd ed., Wiley, Hoboken, New Jersey **2016**.
[2] V. F. McNeill, *Annu. Rev. Chem. Biomol. Eng.* **2017**, *8*, 427.
[3] E. Hettiarachchi, O. Hurab, G. Rubasinghege, *J. Phys. Chem. A* **2018**, *122*, 1291.
[4] E. Hettiarachchi, R. L. Reynolds, H. L. Goldstein, B. Moskowitz, G. Rubasinghege, *Atmos. Environ.* **2019**, *205*, 90.
[5] E. Hettiarachchi, R. L. Reynolds, H. L. Goldstein, B. Moskowitz, G. Rubasinghege, *Atmos. Environ.* **2018**, *187*, 417.
[6] J. Borgatta, A. Paskavitz, D. Kim, J. G. Navea, *Environ. Chem.* **2016**, *13*, 902.
[7] J. Borgatta, J. G. Navea, *WIT Transac. Ecol. Environ.* **2015**, *198*, 155.

[8] H. A. Al-Abadleh, *RSC Adv.* **2015**, *5*, 45785.
[9] H. Fu, D. M. Cwiertny, G. R. Carmichael, M. M. Scherer, V. H. Grassian, *J. Geophys. Res. Atmos.* **2010**, *115*(D11), D11304.
[10] H. Fu, J. Lin, G. Shang, W. Dong, V. H. Grassian, G. R. Carmichael, Y. Li, J. Chen, *Environ. Sci. Technol.* **2012**, *46*, 11119.
[11] J. Mao, S. Fan, L. W. Horowitz, *Environ. Sci. Technol. Lett.* **2017**, *4*, 98.
[12] J. Mao, S. Fan, D. J. Jacob, K. R. Travis, *Atmos. Chem. Phys.* **2013**, *13*, 509.
[13] J. G. Navea, H. Chen, M. Huang, G. R. Carmichel, V. H. Grassian, *Environ. Chem.* **2010**, *7*, 162.
[14] J. G. Navea, E. Richmond, T. Stortini, J. Greenspan, *Langmuir* **2017**, *33*, 10161.
[15] J. D. Schuttlefield, D. Cox, V. H. Grassian, *J. Geophys. Res. Atmos.* **2007**, *112*(D21), D21303.
[16] C. D. Hatch, A. L. Greenaway, M. J. Christie, J. Baltrusaitis, *Atmos. Environ.* **2014**, *87*, 26.
[17] P. J. DeMott, M. D. Petters, A. J. Prenni, C. M. Carrico, S. M. Kreidenweis, J. L. Collett Jr., H. Moosmüller, *J. Geophys. Res. Atmos.* **2009**, *114*, 2156.
[18] C. R. Usher, A. E. Michel, V. H. Grassian, *Chem. Rev.* **2003**, *103*, 4883.
[19] A. E. Michel, C. R. Usher, V. H. Grassian, *Geophys. Res. Lett.* **2002**, *29*, 1665.
[20] P. Galhotra, J. G. Navea, S. C. Larsen, V. H. Grassian, *Energ. Environ. Sci.* **2009**, *2*, 401.
[21] C. J. Ostaszewski, N. M. Stuart, D. M. B. Lesko, D. Kim, M. J. Lueckheide, J. G. Navea, *J. Phys. Chem. A* **2018**, *122*, 6360.
[22] C. Han, W. Yang, Q. Wu, H. Yang, X. Xue, *Environ. Sci. Technol.* **2016**, *50*, 5017.
[23] H. Chen, J. G. Navea, M. A. Young, V. H. Grassian, *J. Phys. Chem. A* **2011**, *115*, 490.
[24] J. G. Navea, M. A. Young, S. Xu, V. H. Grassian, C. O. Stanier, *Atmos. Environ.* **2011**, *45*, 3181.
[25] D. M. B. Lesko, E. M. Coddens, H. D. Swomley, R. M. Welch, J. Borgatta, J. G. Navea, *Phys. Chem. Chem. Phys.* **2015**, *17*, 20775.
[26] J. Schuttlefield, G. Rubasinghege, M. El-Maazawi, J. Bone, V. H. Grassian, *J. Am. Chem. Soc.* **2008**, *130*, 12210.
[27] H. Matsui, N. M. Mahowald, N. Moteki, D. S. Hamilton, S. Ohata, A. Yoshida, M. Koike, R. A. Scanza, M. G. Flanner, *Nat. Commun.* **2018**, *9*, 1.
[28] D. R. Moberg, D. Becker, C. W. Dierking, F. Zurheide, B. Bandow, U. Buck, A. Hudait, V. Molinero, F. Paesani, T. Zeuch, *Proc. Natl. Acad. Sci.* **2019**, *116*, 24413.
[29] Y. Qiu, A. Hudait, V. Molinero, *J. Am. Chem. Soc.* **2019**, *141*, 7439.
[30] J. M. Schiffer, M. Luo, A. C. Dommer, G. Thoron, M. Pendergraft, M. V. Santander, D. Lucero, E. Pecora de Barros, K. A. Prather, V. H. Grassian, R. E. Amaro, *J. Phys. Chem. Lett.* **2018**, *9*, 3839.
[31] J. M. Schiffer, L. E. Mael, K. A. Prather, R. E. Amaro, V. H. Grassian, *ACS Cent. Sci.* **2018**, *4*, 1617.
[32] J. G. Navea, V. H. Grassian, in *Encyclopedia of Interfacial Chemistry: Photochemistry of Atmospheric Particles* (Ed: K. Wandelt), Elsevier, Oxford, UK **2018**, p. 553.
[33] R. Zhang, *Science* **2010**, *328*, 1366.
[34] B. Finlayson-Pitts, J. N. Pitts Jr., *Chemistry of the Upper and Lower Atmosphere: Theory, Experiments, and Applications*, Elsevier; Academic Press, San Diego, CA **1999**.
[35] M. Kulmala, H. Vehkamäki, T. Petäjä, M. Dal Maso, A. Lauri, V.-M. Kerminen, W. Birmili, P. H. McMurry, *J. Aerosol Sci.* **2004**, *35*, 143.
[36] M. Kulmala, J. Kontkanen, H. Junninen, K. Lehtipalo, H. E. Manninen, T. Nieminen, T. Petäjä, M. Sipilä, S. Schobesberger, P. Rantala, A. Franchin, T. Jokinen, E. Järvinen, M. Äijälä, J. Kangasluoma, J. Hakala, P. P. Aalto, P. Paasonen, J. Mikkilä, J. Vanhanen, J. Aalto, H. Hakola, U. Makkonen, T. Ruuskanen, R. L. Mauldin III., J. Duplissy, H. Vehkamäki, J. Bäck, A. Kortelainen, I. Riipinen, T. Kurtén, M. V. Johnston, J. N. Smith, M. Ehn, T. F. Mentel, K. E. J. Lehtinen, A. Laaksonen, V.-M. Kerminen, D. R. Worsnop, *Science* **2013**, *339*, 943.
[37] J. Aitken, *Nature* **1881**, *23*, 384.
[38] W. Kohn, L. Sham, *J. Phys. Rev.* **1965**, *140*, 1133.
[39] W. Kohn, A. D. Becke, R. G. Parr, *J. Phys. Chem.* **1996**, *100*, 12974.
[40] C. Møller, M. S. Plesset, *Phys. Rev.* **1934**, *46*, 618.
[41] S. C. David, H. F. Schaefer, in *Advances in Quantum Chemistry: The Configuration Interaction Method: Advances in Highly Correlated Approaches*, Vol. 34 (Eds: P. Löwdin, J. R. Sabin, M. C. Zerner, E. Brändas), Elsevier; Academic Press, San Diego, CA **1999**, p. 143.
[42] O. Sinanoğlu, *J. Chem. Phys.* **1962**, *36*, 706.
[43] H. Werner, F. R. Manby, P. J. Knowles, *J. Chem. Phys.* **2003**, *118*, 8149.
[44] R. A. DiStasio, Y. Jung, M. Head-Gordon, *J. Chem. Theory Comput.* **2005**, *1*, 862.
[45] G. C. Shields, K. N. Kirschner, *Synth. Reactiv. Inorg. Metal-Org. Nano-Metal Chem.* **2008**, *38*, 32.
[46] R. M. Shields, B. Temelso, K. A. Archer, T. E. Morrell, G. C. Shields, *J. Phys. Chem. A* **2010**, *114*, 11725.
[47] C. Pérez, M. T. Muckle, D. P. Zaleski, N. A. Seifert, B. Temelso, G. C. Shields, Z. Kisiel, B. H. Pate, *Science* **2012**, *336*, 897.
[48] J. O. Richardson, C. Pérez, S. Lobsiger, A. A. Reid, B. Temelso, G. C. Shields, Z. Kisiel, D. J. Wales, B. H. Pate, S. C. Althorpe, *Science* **2016**, *351*, 1310.
[49] A. Tkatchenko, R. A. DiStasio, M. Head-Gordon, M. Scheffler, *J. Chem. Phys.* **2009**, *131*, 094106.
[50] M. B. Goldey, B. Belzunces, M. Head-Gordon, *J. Chem. Theory Comput.* **2015**, *11*, 4159.
[51] E. K. Pokon, M. D. Liptak, S. Feldgus, G. C. Shields, *J. Phys. Chem. A* **2001**, *105*, 10483.
[52] M. B. Day, K. N. Kirschner, G. C. Shields, *Int. J. Quantum Chem.* **2005**, *102*, 565.
[53] B. Temelso, K. L. Klein, J. W. Mabey, C. Pérez, B. H. Pate, Z. Kisiel, G. C. Shields, *J. Chem. Theory Comput.* **2018**, *14*, 1141.
[54] J. Herb, A. B. Nadykto, F. Yu, *Chem. Phys. Lett.* **2011**, *518*, 7.
[55] I. K. Ortega, O. Kupiainen, T. Kurtén, T. Olenius, O. Wilkman, M. J. McGrath, V. Loukonen, H. Vehkamäki, *Atmos. Chem. Phys. Dis.* **2011**, *11*, 27327.
[56] J. Elm, M. Bilde, K. V. Mikkelsen, *J. Chem. Theory Comput.* **2012**, *8*, 2071.
[57] J. Elm, M. Bilde, K. V. Mikkelsen, *J. Phys. Chem. A* **2013**, *117*, 6695.
[58] J. Elm, K. V. Mikkelsen, *Chem. Phys. Lett.* **2014**, *615*, 26.
[59] S. Jiang, Y.-R. Liu, T. Huang, H. Wen, K.-M. Xu, W.-X. Zhao, W.-J. Zhang, W. Huang, *J. Comput. Chem.* **2014**, *35*, 159.
[60] B. Temelso, K. A. Archer, G. C. Shields, *J. Phys. Chem. A* **2011**, *115*, 12034.
[61] M. B. Day, K. N. Kirschner, G. C. Shields, *J. Phys. Chem. A* **2005**, *109*, 6773.
[62] K. N. Kirschner, G. M. Hartt, T. M. Evans, G. C. Shields, *J. Chem. Phys.* **2007**, *126*, 154320.
[63] B. Temelso, G. C. Shields, *J. Chem. Theory Comput.* **2011**, *7*, 2804.
[64] V. Loukonen, T. Kurtén, I. K. Ortega, H. Vehkamäki, A. A. Padua, K. Sellegri, M. Kulmala, *Atmos. Chem. Phys.* **2010**, *10*, 4961.

[65] B. Temelso, T. N. Phan, G. C. Shields, *J. Phys. Chem. A* **2012**, *116*, 9745.
[66] B. von Freyberg, W. Braun, *J. Comput. Chem.* **1991**, *12*, 1065.
[67] A. Rakshit, T. Yamaguchi, T. Asada, P. Bandyopadhyay, *RSC Adv.* **2017**, *7*, 18401.
[68] D. M. Deaven, K. M. Ho, *Phys. Rev. Lett.* **1995**, *75*, 288.
[69] A. Freibert, J. M. Dieterich, B. Hartke, *J. Comput. Chem.* **2019**, *40*, 1978.
[70] U. Buck, C. C. Pradzynski, T. Zeuch, J. M. Dieterich, B. Hartke, *Phys. Chem. Chem. Phys.* **2014**, *16*, 6859.
[71] J. M. Dieterich, B. Hartke, *Mol. Phys.* **2010**, *108*, 279.
[72] B. Hartke, in *Applications of Evolutionary Computation in Chemistry: Application of Evolutionary Algorithms to Global Cluster Geometry Optimization*, Vol. 110 (Ed: R. L. Johnston), Springer, Berlin, Heidelberg, Germany **2004**, p. 33.
[73] R. P. F. Kanters, K. J. Donald, *J. Chem. Theory. Comput.* **2014**, *10*, 5729.
[74] C. W. Padgett, A. Saad, in *Applications of Soft Computing: Genetic Algorithms in Chemistry: Success or Failure is in the Genes*, Vol. 58 (Eds: J. Mehnen, M. Köppen, A. Saad, A. Tiwari), Springer, Berlin, Heidelberg, Germany **2009**, p. 181.
[75] N. Perez-Peralta, M. Contreras, W. Tiznado, J. Stewart, K. J. Donald, G. Merino, *Phys. Chem. Chem. Phys.* **2011**, *13*, 12975.
[76] L. B. Vilhelmsen, B. Hammer, *J. Chem. Phys.* **2014**, *141*, 044711.
[77] B. Temelso, E. F. Morrison, D. L. Speer, B. C. Cao, N. Appiah-Padi, G. Kim, G. C. Shields, *J. Phys. Chem. A* **2018**, *122*, 1612.
[78] T. T. Odbadrakh, A. G. Gale, B. T. Ball, B. Temelso, G. C. Shields, *J. Vis. Exp.* **2020**, *158*, e60964.
[79] J. Zhang, M. Dolg, *Phys. Chem. Chem. Phys.* **2016**, *18*, 3003.
[80] J. Zhang, M. Dolg, *Phys. Chem. Chem. Phys.* **2015**, *17*, 24173.
[81] A. Malloum, J. J. Fifen, Z. Dhaouadi, S. G. N. Engo, N. Jaidane, *Phys. Chem. Chem. Phys.* **2016**, *18*, 26827.
[82] H. Wang, X. Zhao, C. Zuo, X. Ma, F. Xu, Y. Sun, Q. Zhang, *RSC Adv.* **2019**, *9*, 36171.
[83] L. Liu, H. Li, H. Zhang, J. Zhong, Y. Bai, M. Ge, Z. Li, Y. Chen, X. Zhang, *Phys. Chem. Chem. Phys.* **2018**, *20*, 17406.
[84] D. Chen, W. Wang, D. Li, W. Wang, *RSC Adv.* **2020**, *10*, 5173.
[85] Á. González, *Math. Geosci.* **2009**, *42*, 49.
[86] J. V. Kildgaard, K. V. Mikkelsen, M. Bilde, J. Elm, *J. Phys. Chem. A* **2018**, *122*, 5026.
[87] B. Temelso, J. M. Mabey, T. Kubota, N. Appiah-Padi, G. C. Shields, *J. Chem. Inf. Model.* **2017**, *57*, 1045.
[88] G. J. Doyle, *J. Chem. Phys.* **1961**, *35*, 795.
[89] G. P. Ayers, R. W. Gillett, J. L. Gras, *Geophys. Res. Lett.* **1980**, *7*, 433.
[90] R. J. Weber, J. J. Marti, P. H. McMurry, F. L. Eisele, D. J. Tanner, A. Jefferson, *J. Geophys. Res.* **1997**, *102*, 4375.
[91] R. J. Weber, P. H. McMurry, R. L. Mauldin III., D. J. Tanner, F. L. Eisele, A. D. Clarke, V. N. Kapustin, *Geophys. Res. Lett.* **1999**, *26*, 307.
[92] P. H. McMurry, K. S. Woo, R. Weber, D.-R. Chen, D. Y. H. Pui, *Philos. Trans. R. Soc. A* **2000**, *358*, 2625.
[93] M. Kulmala, I. Riipinen, M. Sipilä, H. E. Manninen, T. Petäjä, H. Junninen, M. Dal Maso, G. Mordas, A. Mirme, M. Vana, A. Hirsikko, L. Laakso, R. M. Harrison, I. Hanson, C. Leung, K. J. Lehtinen, V.-M. Kerminen, *Science* **2007**, *318*, 89.
[94] T. Nieminen, H. E. Manninen, S.-L. Sihto, T. Yli-Juuti, R. L. Mauldin, T. Petäjä, I. Riipinen, V.-M. Kerminen, M. Kulmala, *Environ. Sci. Technol.* **2009**, *43*, 4715.
[95] M. Sipilä, T. Berndt, T. Petäjä, D. Brus, J. Vanhanen, F. Stratmann, J. Patokoski, R. L. Mauldin III., A.-P. Hyvärinen, H. Lihavainen, M. Kulmala, *Science* **2010**, *327*, 1243.
[96] J. Kirkby, J. Curtius, J. Almeida, E. Dunne, J. Duplissy, S. Ehrhart, A. Franchin, S. Gangé, L. Ickes, A. Kürten, A. Kupc, A. Metzger, F. Riccobono, L. Rondo, S. Schobesberger, G. Tsagkogeorgas, D. Wimmer, A. Amorin, F. Bianchi, M. Breitenlechner, A. David, J. Dommen, A. Downard, M. Ehn, R. C. Flagan, S. Haider, A. Hansel, D. Hauser, W. Jud, H. Junninen, F. Kreissl, A. Kvashin, A. Laaksonen, K. Lehtipalo, J. Lima, E. R. Lovejoy, V. Makhmutov, S. Mathot, J. Mikkilä, P. Minginette, S. Mogo, T. Nieminen, A. Onnela, P. Pereira, T. Petäjä, R. Schnitzhofer, J. H. Seinfeld, M. Sipilä, Y. Stozhkov, F. Stratmann, A. Tomé, J. Vanhanen, Y. Viisanen, A. Vrtala, P. E. Wagner, H. Walther, E. Weingartner, H. Wex, P. M. Winkler, K. S. Carslaw, D. R. Worsnop, U. Baltensperger, M. Kulmala, *Nature* **2011**, *476*, 429.
[97] F. Riccobono, S. Schobesberger, C. E. Scott, J. Dommen, I. K. Ortega, L. Rondo, J. Almeida, A. Amorim, F. Bianchi, M. Breitenlechner, A. David, A. Downard, E. M. Dunne, J. Duplissy, S. Ehrhart, R. C. Flagan, A. Franchin, A. Hansel, H. Junninen, M. Kajos, H. Keskinen, A. Kupc, A. Kürten, A. N. Kvashin, A. Laaksonen, K. Lehtipalo, V. Makhmutov, S. Mathot, T. Nieminen, A. Onnela, T. Petäjä, A. P. Praplan, F. D. Santos, S. Schallhart, J. H. Seinfeld, M. Sipilä, D. V. Spracklen, Y. Stozhkov, F. Stratmann, A. Tomé, G. Tsagkogeorgas, P. Vaattovaara, Y. Viisanen, A. Vrtala, P. E. Wagner, E. Weingartner, H. Wex, D. Wimmer, K. S. Carslaw, J. Curtius, N. M. Donahue, J. Kirkby, M. Kulmala, D. R. Worsnop, U. Baltensperger, *Science* **2014**, *344*, 717.
[98] E. M. Dunne, H. Gordon, A. Kürten, J. Almeida, J. Duplissy, C. Williamson, I. K. Ortega, K. J. Pringle, A. Adamov, U. Baltensperger, P. Barmet, F. Benduhn, F. Bianchi, M. Breitenlechner, A. Clarke, J. Curtius, J. Commen, N. M. Donahue, S. Ehrhart, R. C. Flagan, A. Franchin, R. Guida, J. Hakala, A. Hansel, M. Heinritzi, T. Jokinen, J. Kangasluoma, J. Kirkby, M. Kulmala, A. Kupc, M. J. Lawler, K. Lehtipalo, V. Markhmutov, G. Mann, S. Mathot, J. Merikanto, P. Meittinen, A. Nenes, A. Onnela, A. Rap, C. L. S. Reddington, F. Riccobono, N. A. D. Richards, M. P. Rissanen, L. Rondo, N. Sarnela, S. Schobesberger, K. Sengupta, M. Simon, M. Sipilä, J. N. Smith, Y. Stozkhov, A. Tomé, J. Tröstl, P. E. Wagner, D. Wimmer, P. M. Winkler, D. R. Worsnop, K. S. Carslaw, *Science* **2016**, *354*, 1119.
[99] L. Yao, O. Garmash, F. Bianchi, J. Zheng, C. Yan, J. Kontkanen, H. Junninen, S. B. Mazon, M. Ehn, P. Paasonen, M. Sipilä, M. Wang, X. Wang, S. Xiao, H. Chen, Y. Lu, B. Zhang, D. Wang, Q. Fu, F. Geng, H. Wang, L. Qiao, X. Yang, J. Chen, V.-M. Kerminen, T. Petäjä, D. R. Worsnop, M. Kulmala, L. Wang, *Science* **2018**, *361*, 278.
[100] B. Temelso, T. E. Morrell, R. M. Shields, M. A. Allodi, E. K. Wood, K. N. Kirschner, T. C. Castonguay, K. A. Archer, G. C. Shields, *J. Phys. Chem. A* **2012**, *116*, 2209.
[101] H. Henschel, J. C. A. Navarro, T. Yli-Juuti, O. Kupiained-Määtä, T. Olenius, I. K. Ortega, S. L. Clegg, T. Kurtén, I. Riipinen, H. Vehkamäki, *J. Phys. Chem. A* **2014**, *118*, 2599.
[102] J. J. Marti, A. Jefferson, X. P. Cai, C. Richert, P. H. McMurry, F. Eisele, *J. Geophys. Res.* **1997**, *102*, 3725.
[103] T. Berndt, O. Böge, F. Stratmann, J. Heintzenberg, M. Kulmala, *Science* **2005**, *307*, 698.
[104] P. Sebastianelli, P. M. Cometto, R. G. Pereyra, *J. Phys. Chem. A* **2018**, *122*, 2116.
[105] P. Sebastianelli, R. G. Pereyra, *Int. J. Quantum Chem.* **2020**, *120*, e26060.

[106] D. J. Bustos, B. Temelso, G. C. Shields, *J. Phys. Chem. A* **2014**, *118*, 7430.
[107] P. Paasonen, T. Olenius, O. Kupiainen, T. Kurtén, T. Petäjä, W. Birmili, A. Hamen, M. Hu, L. G. Huey, C. Plass-Duelmer, J. N. Smith, A. Wiedensohler, V. Loukonen, M. J. McGrath, I. K. Ortega, A. Laaksonen, H. Vehkamäki, V.-M. Kerminen, M. Kulmala, *Atmos. Chem. Phys.* **2012**, *12*, 9113.
[108] S. M. Ball, D. R. Hanson, F. L. Eisele, P. H. McMurry, *J. Geophys. Res.* **1999**, *104*, 23709.
[109] P. Korhonen, M. Kulmala, A. Laaksonen, Y. Viisanen, R. McGraw, J. H. Seinfeld, *J. Geophys. Res.* **1999**, *104*, 26349.
[110] F. Yu, *J. Geophys. Res.* **2006**, *111*, D01204.
[111] W. A. Glasoe, K. Volz, B. Panta, N. Freshour, R. Bachman, D. R. Hanson, P. H. McMurry, C. Jen, *J. Geophys. Res. Atmos.* **2015**, *120*, 1933.
[112] J. Almeida, S. Schobesberger, A. Kürten, I. K. Ortega, O. Kupiainen-Määttä, A. P. Praplan, A. Adamov, A. Amorim, F. Bianchi, M. Breitenlechner, A. David, J. Dommen, N. M. Donahue, A. Downard, E. Dunne, J. Duplissy, S. Ehrhart, R. C. Flagan, A. Franchin, R. Guida, J. Hakala, A. Hansel, M. Heinritzi, H. Henschel, T. Jokinen, H. Junninen, M. Kajos, J. Kangasluoma, H. Keskinen, A. Kupc, T. Kurtén, A. N. Kvashin, A. Laaksonen, K. Lehtipalo, M. Leiminger, J. Leppä, V. Loukonen, V. Makhmutov, S. Mathot, M. J. McGrath, T. Nieminen, T. Olenius, A. Onnela, T. Petäjä, F. Riccobono, I. Riipinen, M. Rissanen, L. Rondo, T. Ruuskanen, F. D. Santos, N. Sarnela, S. Schallhart, R. Schnitzhofer, J. H. Seinfeld, M. Simon, M. Sipilä, Y. Stozhkov, F. Stratmann, A. Tomé, J. Tröstl, G. Tsagkogeorgas, P. Vaattovaara, Y. Viisanen, A. Virtanen, A. Vrtala, P. E. Wagner, E. Weingartner, H. Wex, C. Williamson, D. Wimmer, P. Ye, T. Yli-Juuti, K. S. Carslaw, M. Kulmala, J. Curtius, U. Baltensperger, D. R. Worsnop, H. Vehkamäki, J. Kirkby, *Nature* **2013**, *502*, 359.
[113] J. L. Katz, *J. Chem. Phys.* **1970**, *52*, 4733.
[114] J. Kirkby, J. Duplissy, K. Sengupta, C. Frege, H. Gordon, C. Williamson, M. Heinritzi, M. Simon, C. Yan, J. Almeida, J. Tröstl, T. Nieminen, I. K. Ortega, R. Wagner, A. Adamov, A. Amorim, A.-K. Bernhammer, F. Bianchi, M. Breitenlechner, S. Brilke, X. Chen, J. Craven, A. Dias, S. Ehrhart, R. C. Flagan, A. Franchin, C. Fuchs, R. Guida, J. Hakala, C. R. Hoyle, T. Jokinen, H. Junninen, J. Kangasluoma, J. Kim, M. Krapf, A. Kürten, A. Laaksonen, K. Lehtipalo, V. Makhmutov, S. Mathot, U. Molteni, A. Onnela, O. Peräkylä, F. Piel, T. Petäjä, A. P. Praplan, K. Pringle, A. Rap, N. A. D. Richards, I. Riipinen, M. P. Rissanen, L. Rondo, N. Sarnela, S. Schobesberger, C. E. Scott, J. H. Seinfeld, M. Sipilä, G. Steiner, Y. Stozhkov, F. Stratmann, A. Tomé, A. Virtanen, A. L. Vogel, A. C. Wagner, P. E. Wagner, E. Weingartner, D. Wimmer, P. M. Winkler, P. Ye, X. Zhang, A. Hansel, J. Dommen, N. M. Donahue, D. R. Worsnop, U. Baltensperger, M. Kulmala, K. S. Carslaw, J. Curtius, *Nature* **2016**, *533*, 521.
[115] F. C. Pickard, E. K. Pokon, M. D. Liptak, G. C. Shields, *J. Chem. Phys.* **2005**, *122*, 024302.
[116] F. Pickard, M. E. Dunn, G. C. Shields, *J. Phys. Chem. A* **2005**, *109*, 4905.
[117] T. E. Morrell, G. C. Shields, *J. Phys. Chem. A* **2010**, *114*, 4266.
[118] D. E. Husar, B. Temelso, A. L. Ashworth, G. C. Shields, *J. Phys. Chem. A* **2012**, *116*, 5151.
[119] K. S. Alongi, T. S. Dibble, G. C. Shields, K. N. Kirschner, *J. Phys. Chem. A* **2006**, *110*, 3686.
[120] M. A. Allodi, M. E. Dunn, J. Livada, K. N. Kirschner, G. C. Shields, *J. Phys. Chem. A* **2006**, *110*, 13283.
[121] G. M. Hartt, G. C. Shields, K. N. Kirschner, *J. Phys. Chem. A* **2008**, *112*, 4490.
[122] M. E. Dunn, E. K. Pokon, G. C. Shields, *J. Am. Chem. Soc.* **2004**, *126*, 2647.
[123] A. H. Goldstein, I. E. Galbally, *Environ. Sci. Technol.* **2007**, *41*, 1514.
[124] J. H. Kroll, J. H. Seinfeld, *Atmos. Environ.* **2008**, *42*, 3593.
[125] N. M. Donahue, K. M. Henry, T. F. Mentel, A. Kiendler-Scharr, C. Spindler, B. Bohn, T. Brauers, H. P. Dorn, H. Fuchs, R. Tillmann, A. Wahner, H. Saathoff, K.-H. Nuamann, O. Möhler, T. Leisner, L. Müller, M.-C. Reinnig, T. Hoffmann, K. Salo, M. Hallquist, M. Frosch, M. Bilde, T. Tritscher, P. Barmet, A. P. Praplan, P. F. DeCarlo, J. Dommen, A. S. H. Prévôt, U. Baltensperger, *Proc. Natl. Acad. Sci.* **2012**, *109*, 13503.
[126] B. K. Pun, S. Y. Wu, C. Seigneur, J. H. Seinfeld, R. J. Griffin, S. N. Pandis, *Environ. Sci. Technol.* **2003**, *37*, 3647.
[127] B. B. Palm, P. Campuzano-Jost, A. M. Ortega, D. A. Day, L. Kaser, W. Jud, T. Karl, A. Hansel, J. F. Hunter, E. S. Cross, J. H. Kroll, Z. Peng, W. H. Brune, J. L. Jimenez, *Atmos. Chem. Phys.* **2016**, *16*, 2943.
[128] D. Aljawhary, R. Zhao, A. K. Y. Lee, C. Wang, J. P. D. Abbatt, *J. Phys. Chem. A* **2016**, *120*, 1395.
[129] Z. Finewax, J. A. de Gouw, P. J. Ziemann, *ACS Earth Space Chem.* **2019**, *3*, 1248.
[130] I. J. George, J. P. Abbatt, *Nat. Chem.* **2010**, *2*, 713.
[131] M. Shrivastava, C. D. Cappa, J. Fan, A. H. Goldstein, A. B. Guenther, J. L. Jimenez, C. Kuang, A. Laskin, S. T. Martin, N. L. Ng, T. Petaja, J. R. Pierce, P. J. Rasch, P. Roldin, J. H. Seinfeld, J. Shilling, J. N. Smith, J. A. Thornton, R. Volkamer, J. Wang, D. R. Worsnop, R. A. Zaveri, A. Zelenyuk, Q. Zhang, *Rev. Geophys.* **2017**, *55*, 509.
[132] G. Gambús, P. Patiño, J. Navea, *Energy Fuel.* **2002**, *16*, 172.
[133] L. Bonnet, J.-C. Rayez, *Int. J. Quantum Chem.* **2010**, *110*, 2355.
[134] S. G. Christov, B. Bunsenge, *Phys. Chem.* **1974**, *78*, 537.
[135] R. Castañeda-Arriaga, J. Alvarez-Idaboy, *Int. J. Quantum Chem.* **2012**, *112*, 3479.
[136] B. O. Milhøj, S. P. A. Sauer, *J. Phys. Chem. A* **2015**, *119*, 6516.
[137] H. Chu, W. Wu, Y. Shao, Y. Tang, Y. Zhang, Y. Cheng, F. Chen, J. Lui, J. Sun, *Environ. Sci. Pollut. Res.* **2018**, *25*, 24939.
[138] Y. Zhao, D. G. Truhlar, *J. Chem. Theory. Comput.* **2006**, *2*, 1009.
[139] J. H. Seinfeld, S. N. Pandis, *Atmospheric Chemistry and Physics: From Air Pollution to Climate Change*, 2nd ed., Wiley, New York, NY **2006**.
[140] S. Frka, M. Šala, A. Kroflič, M. Huš, A. Čusak, I. Grgić, *Environ. Sci. Technol.* **2016**, *50*, 5526.
[141] A. Laskin, J. Laskin, S. A. Nizkorodov, *Chem. Rev.* **2015**, *115*, 4335.
[142] V. Purohit, A. K. Basu, *Chem. Res. Toxicol.* **2000**, *13*, 673.
[143] P. M. Esteves, J. Walkimar de Carneiro, S. P. Cardoso, A. G. H. Barbosa, K. K. Laali, G. Rasul, G. K. Prakash, G. A. Olah, *J. Am. Chem. Soc.* **2003**, *125*, 4836.
[144] J. M. Andino, J. N. Smith, R. C. Flagan, W. A. Goddard, J. H. Seinfeld, *J. Phys. Chem.* **1996**, *100*, 10967.
[145] J. D. Surratt, A. W. H. Chan, N. C. Eddingsaas, M. Chan, C. L. Loza, A. J. Kwan, S. P. Hersey, R. C. Flagan, P. O. Wennberg, J. H. Seinfeld, *Proc. Natl. Acad. Sci.* **2010**, *107*, 6640.
[146] Y. Lin, H. Zhang, H. O. T. Pye, Z. Zhang, W. J. Marth, S. Park, M. Arashiro, T. Cui, S. H. Budisulistiorini, K. G. Sexton, W. Vizuete, Y. Xie, D. J. Luecken, I. R. Piletic, E. O. Edney, L. J. Bartolotti, A. Gold, J. D. Surratt, *Proc. Natl. Acad. Sci.* **2013**, *110*, 6718.
[147] Y. Lin, Z. Zhang, K. S. Docherty, H. Zhang, S. H. Budisulistriorini, C. L. Rubitschun, S. L. Shaw, E. M. Knipping, E. S. Edgerton, T. E. Kleindienst, A. Gold, J. D. Surratt, *Environ. Sci. Technol.* **2012**, *46*, 250.

[148] T. Sun, Y. Wang, C. Zhang, X. Sun, W. Wang, *Atmos. Environ.* **2011**, *45*, 1725.
[149] C. Tong, M. Blanco, W. A. Goddard, J. H. Seinfeld, *Environ. Sci. Technol.* **2006**, *40*, 2333.
[150] J. W. DePalma, A. J. Horan, W. A. Hall IV., M. V. Johnston, *Phys. Chem. Chem. Phys.* **2013**, *15*, 6935.
[151] J. Xu, B. Finlayson-Pitts, R. B. Gerber, *J. Phys. Chem. A* **2017**, *121*, 2377.
[152] H. Chen, M. J. Ezell, K. D. Arquero, M. E. Varner, M. L. Dawson, R. B. Gerber, B. J. Finlayson-Pitts, *Phys. Chem. Chem. Phys.* **2015**, *17*, 13699.
[153] S. Patai Ed., *Sulphinic Acids, Esters and Derivatives*, Wiley, Chichester, UK **1990**.
[154] M. D. Liptak, G. C. Shields, *Int. J. Quantum Chem.* **2001**, *85*, 727.
[155] D. M. Cwiertny, M. A. Young, V. H. Grassian, *Annu. Rev. Phys. Chem.* **2008**, *59*, 27.
[156] G. Rubasinghege, V. H. Grassian, *J. Phys. Chem. A* **2009**, *113*, 7818.
[157] K. K. Irikura, R. D. Johnson, R. N. Kacker, *J. Phys. Chem. A* **2005**, *109*, 8430.
[158] D. Kim, Y. Xiao, R. Karchere-Sun, E. Richmond, H. M. Ricker, A. Leonardi, J. G. Navea, *ACS Earth Space Chem.* **2020**, *4*(5), 750. https://pubs.acs.org/doi/10.1021/acsearthspacechem.0c00057.
[159] H. Chen, C. E. Nanayakkara, V. H. Grassian, *Chem. Rev.* **2012**, *112*, 5919.
[160] C. George, M. Ammannm, B. D'Anna, D. J. Donaldson, S. A. Nizkorodov, *Chem. Rev.* **2015**, *115*, 4218.
[161] V. P. Indrakanti, J. D. Kubicki, H. H. Schobert, *Energy Fuel.* **2008**, *22*, 2611.
[162] J. M. H. Lo, T. Ziegler, P. D. Clark, *J. Phys. Chem. C* **2010**, *114*, 10444.
[163] M. Martins-Costa, J. M. Anglada, J. S. Francisco, M. F. Ruiz-López, *J. Am. Chem. Soc.* **2018**, *140*, 12341.
[164] J. A. Adame, L. Lope, M. Sorribas, A. Notario, M. Yela, *Sci. Total Environ.* **2020**, *716*, 137075.
[165] A. P. Cuesta-Mosquera, M. Wahl, J. G. Acosta-López, J. A. García-Reynoso, B. H. Aristizábal-Zuluaga, *Sustain. Cities Soc.* **2020**, *52*, 101852.
[166] J. Jiang, Y. Zha, L. Li, *Atmos. Pollut. Res.* **2019**, *10*, 913.
[167] Z. Qu, D. K. Henze, C. Li, N. Theys, Y. Wang, J. Wang, W. Wang, J. Han, C. Shim, R. R. Dickerson, X. Ren, *J. Geophys. Res. Atmos.* **2019**, *124*, 8336.
[168] H. Zhao, X. Sheng, S. Fabris, D. R. Salahub, T. Sun, L. Du, *J. Chem. Phys.* **2018**, *149*, 194703.
[169] Z. Yu, M. Jang, J. Park, *Atmos. Chem. Phys.* **2017**, *17*, 10001.
[170] S. Benkoula, O. Sublemontier, M. Patanen, C. Nicolas, F. Sirotti, A. Naitabdi, F. Gaie-Levrel, E. Antonsson, D. Aureau, F. Ouf, S. Wada, A. Etcheberry, K. Ueda, C. Miron, *Sci. Rep.* **2015**, *5*, 15088.
[171] R. L. Kurtz, R. Stock-Bauer, T. E. Msdey, E. Román, J. D. Segovia, *Surf. Sci.* **1989**, *218*, 178.
[172] S. Wendt, R. Schaub, J. Matthiesen, E. K. Vestergaard, E. Wahlström, M. D. Rasmussen, P. Thostrup, L. M. Molina, E. Lægsgaard, I. Stensgaard, B. Hammer, F. Besenbacher, *Surf. Sci.* **2005**, *598*, 226.
[173] H. A. Al-Abadleh, V. H. Grassian, *Langmuir* **2003**, *19*, 341.
[174] C. M. Archuleta, P. J. DeMott, S. M. Kreidenweis, *Atmos. Chem. Phys.* **2005**, *5*, 2617.
[175] C. D. Hatch, J. S. Wiese, C. C. Crane, K. J. Harris, H. G. Kloss, J. Baltrusaitis, *Langmuir* **2012**, *28*, 1790.
[176] G. Rubasinghege, V. H. Grassian, *Chem. Commun.* **2013**, *49*, 3071.
[177] J. Baltrusaitis, J. D. Schuttlefield, E. Zeitler, J. H. Jensen, V. H. Grassian, *J. Phys. Chem. C* **2007**, *111*, 14870.
[178] J. Baltrusaitis, J. Schuttlefield, J. H. Jensen, V. H. Grassian, *Phys. Chem. Chem. Phys.* **2007**, *9*, 4970.
[179] N. V. Karimova, M. Luo, V. H. Grassian, R. B. Gerber, *Phys. Chem. Chem. Phys.* **2020**, *22*, 5046.
[180] G. C. Shields, *Int. J. Quantum Chem.* **2020**, e26274.
[181] G. C. Shields, *SPUR* **2019**, *3*, 5.

AUTHOR BIOGRAPHIES

Angelina Leonardi is a native of Colorado. She is a senior at Skidmore College majoring in chemistry with a French minor. She has been working in the Physical Chemistry Research Laboratory at Skidmore for 3 years, where she studies atmospheric photosensitization reactions, the functionalization of inert hydrocarbons via oxygen plasma, and the atmospheric fate of combustion particles. She has a strong interest in quantum mechanics and plans to pursue the Ph.D. degree in atmospheric physical chemistry in 2021.

Heather M. Ricker is currently pursuing chemistry and environmental studies and sciences at Skidmore College. In 2019, she joined the Atmospheric Physical Chemistry Laboratory led by Dr Juan Navea at Skidmore, and has worked on heterogeneous photochemistry projects, including studies of the daytime mechanisms of nitrous acid formation and the photodegradation of nitrites. Her research interests include the physical chemistry of environmental processes and disruptors, and the application of chemistry in environmental solutions.

Ariel G. Gale is a Furman University alumni and is currently a PhD student at Emory University. She is majoring in chemistry and minoring in women's and gender studies. She went to high school in Knoxville, Tennessee, before joining the research group of Prof. George C. Shields. Since then, she has focused her research efforts on prebiotic chemistry for over 2 years. She has been a recipient of the Barry M. Goldwater and Beckman scholarships. She plans to attend the graduate school to pursue the Ph.D. degree.

Benjamin T. Ball attended high school at Mountain Heritage High School, Burnsville, North Carolina. He is currently pursuing a Masters at Furman University in computational chemistry at the Department of Chemistry. He joined the research group of Prof. George C. Shields in the summer of 2018 and completed 2 years of research. His work focuses on the thermodynamics of the hydration of sulfuric acid and various amino acids in the atmosphere.

Tuguldur T. Odbadrakh received the B.S. degree in Chemistry from West Virginia University, where he worked in the research group of Prof. Xiaodong Shi. He then joined the research group Prof. Kenneth Jordan at the University of Pittsburgh for graduate studies. There he studied the effects of hydration on an excess proton. He then joined the research group of Prof. George Shields at Furman University, where he is currently a postdoctoral fellow.

George C. Shields is a native of Marcellus, NY. He received his degrees from Georgia Tech, and was a postdoctoral fellow with Prof. Thomas Steitz at Yale University. He was a recipient of the 2015 ACS award for Research at an Undergraduate Institution, the RCSA 2018 Transformational Research and Excellence in Education award, and the 2020 CUR Fellows award. He was elected a Fellow of AAAS in 2019. Prof. Shields is the director of MERCURY, the Molecular Education and Research Consortium in Undergraduate Computational ChemistRY.

Juan G. Navea is an Associate Professor of Chemistry at Skidmore College. He received the B.S. degree from Universidad Central de Venezuela, and the Ph.D. from Baylor University. He was a postdoctoral fellow with Prof. Vicki H. Grassian at the University of Iowa. He combines theory and experiments to investigate heterogeneous chemistry and photochemistry in the atmosphere. Dr Navea has mentored over 50 undergraduates in theoretical and experimental methods. He joined the MERCURY consortium in 2016.

How to cite this article: Leonardi A, Ricker HM, Gale AG, et al. Particle formation and surface processes on atmospheric aerosols: A review of applied quantum chemical calculations. *Int J Quantum Chem*. 2020;e26350. https://doi.org/10.1002/qua.26350